BILINGUAL PUBLISHING CO.
Pioneer of Global Academics Since 1984

Journal of Building Material Science

Volume 4 • Issue 1 • June 2022 ISSN 2630-5216(Online)

BILINGUAL PUBLISHING CO.
Pioneer of Global Academics Since 1984

Volume 4 Issue 1 • June 2022 • ISSN 2630-5216 (Online)

Journal of Building Material Science

BILINGUAL PUBLISHING CO.
Pioneer of Global Academics Since 1984

BILINGUAL PUBLISHING CO.
Pioneer of Global Academics Since 1984

Volume 4 | Issue 1 | June 2022 | Page1-53
Journal of Building Material Science

Contents

Articles

BILINGUAL PUBLISHING CO.
Pioneer of Global Academics Since 1984

Journal of Building Material Science
https://ojs.bilpublishing.com/index.php/jbms

ARTICLE

Characteristics of Ordinary Portland Cement Paste Containing Rice Husk Ash and Conplast [SP 430]

Elinwa, Augustine Uchechukwu[1*] Olakunle Johnson Olomi[2] Duna, Samson[1]

1. Civil Engineering Department, Abubakar Tafawa Balewa University, Bauchi, Nigeria
2. Works Department, University of Jos Teaching Hospital JUTH, Jos, Nigeria

ARTICLE INFO

Article history
Received: 25 November 2021
Accepted: 20 December 2021
Published Online: 10 January 2022

Keywords:
Rice husk ash
Conplast SP 430
Paste characteristics
Statistics
Linear regression

ABSTRACT

An experimental investigation on rice husk ash (RHA) and Conplast SP 430 (CP-admixture) was carried out to evaluate their effects on the paste characteristics (soundness, consistency, initial and final setting times). The cement content used was 300g and the brand was 'Ashaka' Portland cement conforming to BS EN 12 1973. Various combinations of the mixtures OPC-RHA-CP-admixture were used to establish performance characteristics of the pastes. Statistical characteristics, and linear regression models (no-transformation, $\lambda = 0.5$, and Box-Cox transformation) were developed on the experimental data for decisions on their performances.

1. Introduction

Nigeria produces approximately 4.3 million tons of rice paddy per year. The waste which is the husk has an approximate volume of 1.1 to 2 million tons per year [1,2]. These wastes can translate to tremendous wealth if properly and economically utilized mostly in our construction industry. In cement technology, this material is classified as a supplementary cementing material (SCM) or cement replacement material (CRM), as the case may be. It is also characterized as a low grade material. One of the setbacks in the use of these low grade materials is the lack of appropriate technology in processing, and the proper knowledge of its behavior when used as a composite. In this research the focus is on rice husk ash. The technology in the use of SCMs/CRMs is still at the teething stage in Africa and most specifically, Nigeria. The studies on the SCMs/CRMs have concentrated mostly on concrete oblivious of the fact that the paste in the concrete constitutes 10 to 15 % of the total concrete

*Corresponding Author:
Elinwa, Augustine Uchechukwu,
Civil Engineering Department, Abubakar Tafawa Balewa University, Bauchi, Nigeria;
Email: auelinwa@gmail.com

DOI: https://doi.org/10.30564/jbms.v4i1.4144

volume, and the weakest point of attack by infiltrating chemicals. The quality of the paste determines the character of the concrete. The strength of the paste, in turn depends on the ratio of water to cement. Therefore, it is very important that the characteristics of the paste is known and the processes for durable paste constituent standards strictly applied. Darweesh [3] worked on the use of black liquor waste as cement admixture or cement and concrete admixtures. Some of his conclusions showed that the water of consistency was increased by 1.68 % to 13.12 % with OPC, and by 4.11 % to 13.85 % with LPC, in comparison with those of their planks. On the other hand, the PBL waste decreased the setting times (initial or final) with either OPC or LPC. With 3 % PBL the initial and final setting times decreased from 140 to 119 min and decreased from 255 to 231 min with OPC. With LPC pastes, these changes were from 148 to 128 min and from 266 to 148 min. He therefore, concluded that setting was faster with OPC than with LPC. Hence, PBL waste can act as an accelerator for cement pastes. Habeeb and Mahmud [4] and Abubakar [2] both worked on RHA. Dobiszewska and Beycioğlu [5] researched on waste basalt powder, while Samantasngha and Singh [6] was on slag blended geopolymer paste and mortar. Understanding the underlying mechanisms of the working of these cementitious pastes are key to optimize and transit the technology to the Nigerian construction industry.

Table 1 is a collection of literature of works on paste characteristics of different types of SCMs/CRMs with and without admixtures. The collections in Table 1 show that vital information on the paste, such as cement content, water quantity or water-cementitious materials, etc. used were omitted, and therefore, points to many inherent gaps in our experiential methods and omissions of important steps. Abubakar [2] for instance, mentioned consistency as a subtitle but never highlighted anything on it. Consistency is the water affinity of the material, and very important in the classification of the material. These are some of the gaps addressed in this work. Good experimental procedures that adheres to proper code interpretations and specifications, coupled with good documentations of procedures will boost confidence in the use of these lower grade materials. The study is on the paste characteristics of rice husk ash (RHA) and Conplast SP 430 [7] which are low grade materials. It is very important the RHA and CP-admixture with cement after setting, shall not undergo any appreciable change of volume to cause disruption of set and hardened mass. If this is allowed, it may cause serious difficulties for the durability of structures when such cementitious materials are used. The paste characteristics considered are soundness, consistency, and initial and final setting times. They were carried out experimentally with RHA as replacement materials in proportions of 0, 10, 20, 30, 40 and 50 % by wt. % of cement, and CP-admixture, at 5.7 mL by wt. % of cement to produce OPC-RHA-CP pastes.

Table 1. Tabulation of Past Research Results on Paste Characteristics

Researcher	Year	**Material**	**Repl. (%)**	**Mix**					**Paste Characteristics**			
				Cement (g)	Cement Type	Water (kg/m^3)	Admixture Type	Dosage	Sdness (mm)	Contcy (%)	Initial Setting (min)	Final Setting (min)
Elinwa and Mahmood [8]	2002	Sawdust ash	0	Not Specified	Ashaka Portland cement	*0.32	Nil	Nil	0.70	-	116	241
			5			*0.32			0.75	-	118	247
			10			*0.34			1.00	-	128	1267
			15			*0.35			1.15	-	135	283
			20			*0.37			1.25	-	160	298
			25			*0.39			1.30	-	170	318
			30			*0.42			1.45	-	190	337
Samantasinghar and Singh [6]	2019	GGBS	0	Not specified		Not specified	NaOH	16 M		39	700	1525
			20							38	180	400
			40							36	80	100
			60							34	50	80
			80							32	25	50
			100							31	20	20
Alkheder et al [9]	2016	Olive waste husk	0	Not specified		165.0					160.8	378
			3			161.2					181.9	380
			6			159.1					210.3	383
			9			156.3					221.6	387
			12			152.2					227.4	389
			15			148.6					231.0	391

Researcher	Year	Material	Repl. (%)	Mix					Paste Characteristics			
				Cement (g)	Cement Type	Water (kg/m^3)	Admixture Type	Dosage	Sdness (mm)	Contcy (%)	Initial Setting (min)	Final Setting (min)
Mbugua et al [10]	2016			500g			Gum Arabic	0			180	250
								0.3			310	490
								0.4			340	500
								0.5			390	590
								0.6			210	605
								0.7			150	600
								0.8			240	500
								0.9			100	495
								1.0			90	490
Mbugua et al [10]	2016			500g			Tard CE (Commercial)	0			180	250
								0.3			440	660
								0.4			400	790
								0.5			330	795
								0.6			325	796
								0.7			320	800
Dobiszewska and Beyciolu [5]	2017	Basalt powder	0		CEM 142R	*0.5				29	140	174
			1								150	167
			2								142	225
			3								164	225
			4								146	228
			6								164	249
			8								166	232
			10								170	265
Dobiszewska and Beyciolu [5]	2017	Basalt powder	0		CEM II/ A-S425R	*0.5				27	188	272
			1								193	276
			2								190	288
			3								186	287
			4								190	289
			6								201	291
			8								203	296
			10								202	311
Dobiszewska and Beyciolu [5]	2017	Basalt powder	0		CEMII/ A-V425R	*0.5				27	221	311
			1								230	305
			2								226	310
			3								226	308
			4								235	288
			6								192	302
			8								203	330
			10								246	324
Dobiszewska and Beyciolu [5]	2017	Basalt powder	0		CEM II/ B-V325R	*0.5				28	215	322
			1								205	329
			2								200	344
			3								220	335
			4								225	340
			6								218	353
			8								236	349
			10								232	372
Dobiszewska and Beyciolu [5]	2017	Basalt powder	0		CEM II/ B-V425N	*0.5				30	191	246
			1								185	252
			2								180	258
			3								207	253
			4								205	260
			6								192	267
			8								207	265
			10								202	262

Researcher	Year	Material	Repl. (%)	Mix					Paste Characteristics			
				Cement (g)	Cement Type	Water (kg/m^3)	Admixture Type	Dosage	Sdness (mm)	Contcy (%)	Initial Setting (min)	Final Setting (min)
Elinwa, AU [11]	2016	Hospital waste ash	0	Not given	Ashaka Portland cement				12.2	29	45	496
			10						11.0	34	185	876
			20						9.6	36	300	985
			30						11.3	39	490	1075
			40						13.3	41	690	11000
Elinwa and Abdulrazaaq [12]	2020	PVC powder	0	300	OPC					32.5	90	190
			5							32.8	96	253
			10							33.2	99	271
			20							34.0	105	280
			30							36.8	108	290
			40							39.5	113	300

2. Materials

The materials used are Ashaka Portland cement, rice husk ash and Conplast SP 430 as the plasticizer. The cement conforms to BS EN 197 Part 1 [13], and was procured at the local market in Bauchi, Nigeria. The rice husk ash used for the production of the ash was collected as a waste threshed out and separated from the rice grains. Therefore, it was collected as a waste and calcined in the kiln of the Industrial Department of the university at a temperature range of 400 ^oC to 600 ^oC, grinded using pestle and mortar, and sieved using a sieve size of 150 µm. The physical and chemical properties were carried out in accordance with ASTM C 618-12 [14]. The cement chemical properties were tested at Ashaka Cement Company in Ashaka, Gombe State. The physical and chemical properties of the 'Ashaka' OPC and RHA are shown in Table 2.

Table 2. Physical and Chemical Properties of Ashaka Portland Cement and Rice Husk Ash

Parameter	Cement	Rice Husk Ash
Physical Properties		
Specific gravity	3.12	1.934
Fineness (kg/m^2)	330	20.2 (%)
Bulk density (kg/m^3) [ref]	830-1650	
Consistency (%)	29	
Initial setting time (min)	65	
Final setting time (min)	275	
Soundness (mm)	2.5	
LOI	-	7.0
Chemical Properties		
SiO_2	19.68	73.97
Al_2O_3	6.44	7.03
Fe_2O_3	3.32	1.19
CaO	60.92	0.96
MgO	0.97	2.45
SO_3	2.28	3.14
K_2O	0.85	2.78
Na_2O	0.12	0.90
TiO_2	0.30	Nil
P_2O_5	0.20	6.18
Mn_2O_3	0.20	1.40

The superplasticizer used is Conplast SP 430 [7] and conforms to ASTM-C-494-92 [15]. The extracts from the manufactures literature describes it as a chloride free, superplasticizing admixture based on selected sulphonated naphthalene polymers. It is a brown solution and disperses in water. It is suitable for use with all types of Portland cements and cement replacement materials such as rice husk ash. Table 3 shows the typical properties of Conplast SP 430.

Table 3. Typical Properties of Conplast SP 430

Parameter	Description
Appearance	Brown liquid
Specific gravity	1.18 @ 25oC
Chloride content	Nil to BS 5075/BS: EN934
Air entrainment	Less than 2 % additional air is entrained at normal dosages

3. Experiment

The soundness, standard consistency and initial and final setting times were carried out using ordinary Portland cement (OPC) paste containing rice husk ash (RHA) and Conplast SP 430 (CP-admixture) in proportions of 0, 10, 20, 30, 40, and 50 %, respectively. The control mix was designated as MR-00, reflecting a paste without RHA or CP-admixture. The other paste compositions are labelled as MR-10/50 for OPC-pastes containing RHA only, and MRCP-10/50 for OPC-pastes containing both RHA and CP, respectively. A cement content of 300 g was used with RHA replacements of cement by wt. %, and/or, with a CP-admixture dosage of 5.7 mL wt. % of cement. These mixes were used to study their effects on the soundness, consistency and initial and final setting times.

Soundness of cement is a quality assurance test of cement. This was carried out to examine expansion due to the presence of free lime and magnesia (MgO) in the cement. This is important to affirm that the cement after setting shall not undergo a large expansion to cause

disruption of the cement used. It was carried out using the Le-Chateliers apparatus and consists of a small split cylinder of spring brass to other non-corrodible metal of 0.5 mm thickness forming a mold of 30 mm internal diameter and 30 mm high. On either side of the split, two indicators are brazed suitably with pointed ends made of 2 mm diameter brass wire in such a way that the distance of these ends to the centre of the cylinder is 165 mm. The split cylinder was kept between two glass plates and the temperature in the laboratory was almost 29°C, and the relative humidity was 62 %. The immersed Le-Chatelier molds were raised to a temperature of approximately 27 °C, and measured with a Vernier caliper.

The consistency of a binder paste is the measure of the degree of wetness or fluidity of the prepared paste. The objective of conducting this test is to find out the amount of water needed to be added to the cement to get a paste of normal consistency. It is defined as that consistency that will permit the Vicat plunger to penetrate to a point 5 to 7 mm from the bottom of the Vicat mold. Pastes with the above compositions were used for this test. The precaution taken was that gauging was kept below 5 min to avoid setting before time. The test was conducted in accordance with BS 4550: 1978 [16] specification, and evaluated using Equation (1):

$$Standard\ Consistency\ (\%) = \frac{Weight\ of\ water\ added}{Weight\ of\ cementitious\ material}\ x\ 100 \quad (1)$$

The initial setting time is the time when cement paste starts hardening while the final setting time is the time when cement paste has hardened sufficiently in such a way that a 1 mm needle makes an impression on the paste in the mold but 5 mm needle does not make any impression. Setting time is the is the time required for stiffening of cement paste to a defined consistency., and thus initial setting time is important for transportation, placing and compaction of cement concrete. It is required to delay the process of hydration or hardening. The Vicat's apparatus was used for this test and conducted in accordance with BS 12: [1] and BS 4550 [16] specifications respectively. The initial and final setting times are calculated as:

$$Initial\ Setting\ Time = T_2 - T_1$$
$$Final\ Setting\ Time = T_3 - T_1 \quad (2)$$

Where,

T_1= Time at which water was first added to cement

T_2= Time when needle failed to penetrate 5 mm to 7 mm from bottom of the mold

T_3= Time when the needle made an impression but the attachment failed to do so.

The results of the soundness, consistency and initial and final times of setting are shown in Table 4.

Table 4. Soundness, Consistency and Setting Times of RHA-CP-OPC Paste

Mix No	Conplast (mL)	Soundness (mm)	Consistency (%)	Setting Times (Min)	
				Initial	Final
MR-00	Nil	7.0	36.0	120.0	180.0
MR-10	Nil	8.0	39.0	130.0	219.0
MR-20	Nil	8.0	55.0	152.0	249.0
MR-30	Nil	10.0	58.0	160.0	271.0
MR-40	Nil	10.0	101.0	210.0	345.0
MR-50	Nil	10.0	112.0	276.0	397.0
MRCP-00	5.7	9.0	34.0	128.0	186.0
MRCP-10	5.7	9.3	37.0	137.0	225.0
MRCP-20	5.7	9.7	50.0	159.0	258.0
MRCP-30	5.7	9.9	55.0	166.0	278.0
MRCP-40	5.7	9.8	60.0	216.0	352.0
MRCP-50	5.7	9.5	65.0	284.0	405.0

Table 5. Percentage Difference of OPC-RHA-CP Paste

Mix-Combination	Replacement (%)	Soundness (mm)	Consistency (%)	Initial Setting	Final Setting
Control Paste with Control with CP (MR-00 and MRCP-00) – ***Mix 0***	0.00	28.6	-5.6	6.7	3.3
Control paste and Paste with RHA (MR-00 and MR-10, 20, etc) – ***Mix 1***	10	14.3	8.3	8.3	21.7
	20	14.3	52.8	26.7	38.3
	30	42.9	61.0	33.3	50.6
	40	42.9	180.6	75.0	91.7
	50	42.9	211.1	130.0	120/6
Control Paste with CP and RHA with CP (MRCP-00 and MRCP-10, 20, etc) – ***Mix 2***	10	3.3	8.8	7.0	21.0
	20	7.8	47.1	24.2	37.7
	30	10.0	61.8	29.7	49.5
	40	8.9	76.5	68.8	89.2
	50	5.6	91.2	121.9	117.7
Paste with RHA and RHA paste with CP (MR-10, 20, … and MRCP-10, 20, etc) – ***Mix 3***	10	16.3	-5.1	5.4	2.7
	20	21.3	-10.0	4.6	3.6
	30	-1.0	-5.5	3.8	2.6
	40	-2.0	-40.6	2.9	2.0
	50	-5.0	-42.0	2.9	2.0

4. Discussion

What gives cement it's property is the CaO content and it has a cementing property. This is approximately 61 %. The SiO_2 in the cement is only approximately 20 %. However, for the RHA the SiO_2 is 74 % and the CaO is just approximately 1 %. The sum of the SiO_2 + Al_2O_3 + Fe_2O_3 in the RHA is approximately 82 %, which is greater

than the 70 % specified in ASTM for pozzolanicity. The limits of the MgO and Na_2O both in the cement and RHA are 0.97/0.12 and 2.43/0.90. These are both less than the limits set for them by BS 12 (1999), that is 0.1 to 4.0 and 0.2 to 1.3, respectively. Can be said to be okay. The K_2O content and the LOI are 2.8 % and 7 % respectively. A well burnt RHA has an average composition 2 % K_2O and 5 % carbon (LOI). Therefore, within the experimental errors the RHA can be said to be okay.

Figures labeled 3a and 4a are plots of the data on paste characteristics of the OPC-RHA-CP-admixture cement paste, while Figures 3b and 4b are plots taken from Table 5 showing the percentage differences recorded for each mix combinations (***Mix 0 to Mix 3***). The performances of these pastes reflect the characteristics of the RHA which are dependent on three factors: (i) the composition of the rice husk, (ii) the burning temperature and, (iii) the burning time. Under controlled burning conditions (as in this case) the volatile organic matter in the rice husk consisting of cellulose and lignin are removed and the residual ash is predominantly amorphous silica with a (microporous) cellular structure as shown in Figures 1 and 2, the microstructure and diffractogram of the RHA.

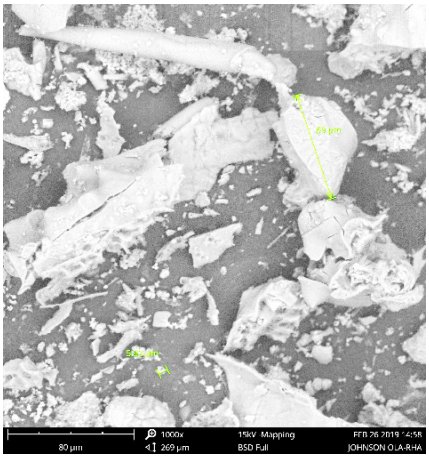

Figure 1. Micrograph of RHA

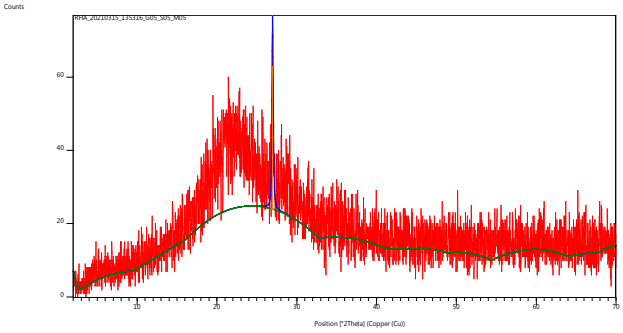

Figure 2. XRD Diffractograme of RHA

The soundness of the OPC-RHA-CP paste is shown in Figure 3. It shows that for all combinations of the paste the soundness was ≤ 10 %. Therefore, it can be said that the addition of RHA and/or CP-admixture to OPC paste will not cause unsoundness and after setting will not undergo any appreciable change of volume. The addition of 5.7 mL of CP-admixture by wt. % of cement to OPC increased the soundness by approximately 28 %. The difference between the control mix (MR-00) and the mix containing RHA (MR-10 to MR-50) without CP-admixture showed an increase of 14.3 % at 10 and 20 % replacements respectively, and remained constant at 42.9 % at 30 to 50 % replacements. The same comparison is made for the case when the control paste containing CP-admixture (MRCP-00) and that containing RHA with CP-admixture (MRCP-10 to MRCP-50). The comparison shows increases of 3.3 at 10 % with a peak value of 10 % at 30 % replacement, and fell to a value of 5.6 % at 50 % replacement. However, the case of adding CP-admixture to MR-00 and MR-10 to MR-50, and compared shows that it has drastic effects at higher replacement levels of RHA. At 10 t0 20 % replacements there were increases of 16. 3 and 21.3 % respectively, but drastically reduced from 30 to 50 % replacements to -1.0 to -5.0 %.

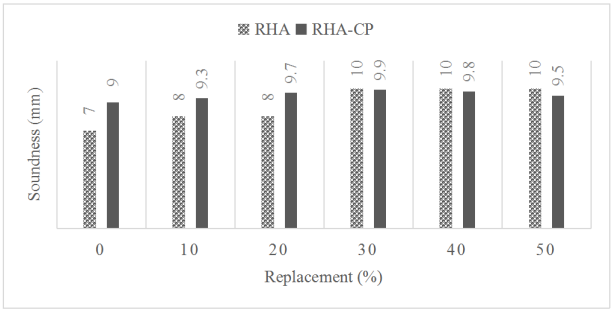

(a) Soundness Plot

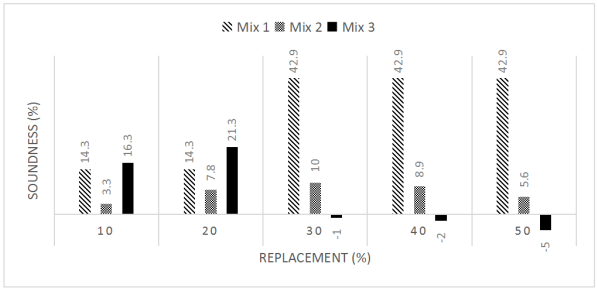

(b) Soundness Difference

Figure 3. Soundness of RHA-CP-OPC Paste

Figure 4 is the consistency of OPC-RHA-CP cement paste. The consistency is the water affinity of the cementitious material. This decreased by 5.6 % when CP-admixture was added to the control mix (MR-00).

One of the advantages of water reducing admixture such as naphthalene sulphonated is that it reduces the water-cementitious ratio while keeping the concrete workable. For the mix without the CP-admixture (MR-00 and MR-10 to MR-50) the water requirement increased from 8.3 to 211.1 %. RHA contains a cellular, honeycomb morphology of amorphous silica and this morphology results in high water absorption. Therefore, the increase in water affinity can be attributed to this rough texture and amorphous nature of the RHA. We therefore, need more water for workability. This behavior is further confirmed for the same mix but with CP-admixture (MRCP-00 and MRCP-10 to MRCP-50 where the water for workable OPC paste decreased from 8.8 to 91.2 %.

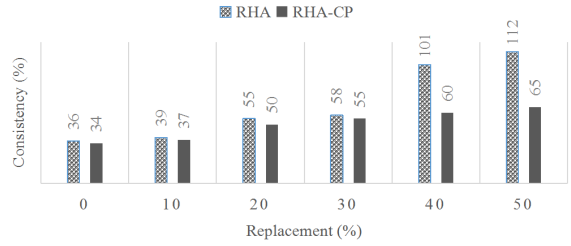

(a) Consistency Plot

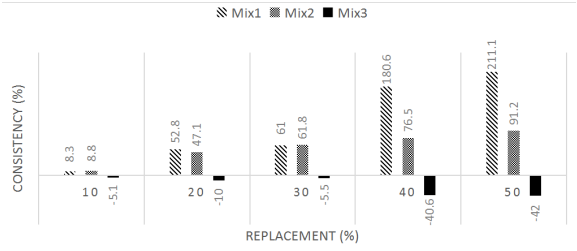

(b) Percentage Difference

Figure 4. Consistency of RHA-CP-OPC Paste

The situations with the initial and final setting times are not different (Figures 5a and 5b) and (Figures 6a and 6b), respectively. Both the RHA and CP-admixture increased the setting times in various degrees as shown. It therefore goes to show that these materials are retarders. Retarders are useful additives especially for hot weather concreting. This, also advances one of the characteristics of the CP-admixture that it improves cohesion, and particle dispersion minimizes segregation and bleeding with increased workability.

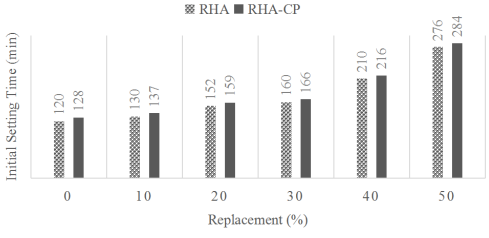

(a) Initial Setting Time Plot

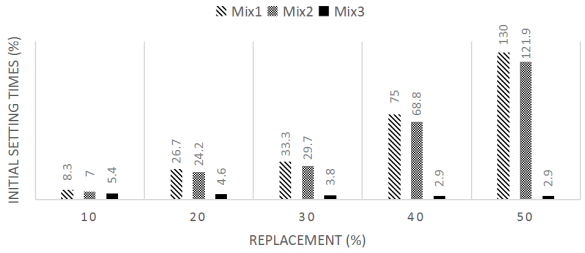

(b) Percentage Difference

Figure 5. Initial Setting Time of RHA-CP-OPC Paste

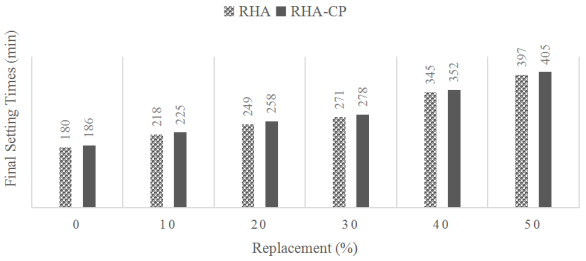

(a) Final Setting Time Plot

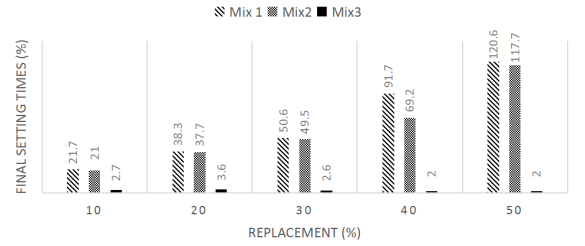

(b) Final Setting Time Difference

Figure 6. Final Setting Time of RHA-CP-OPC Paste

Statistical Characteristics and Linear Regression Model of OPC-RHA-CP Paste

Table 6 shows the statistical characteristics of the paste. It shows the mean, standard deviation etc of the paste. The mean value characterizes the central tendency or location of the data, while the coefficient of variation provides a general feeling about the performance of the method. It is the distribution of data points in a data series around the mean and thus, expresses the variation as a percentage of the mean. The larger the coefficient of variation, the greater the spread in the data. The standard error of the mean (SE Mean) estimates the variability between sample means, and the standard deviation and thus, establishes a benchmark for estimating the overall variation of a process. Whereas the standard error of the mean estimates the variability between samples, the standard deviation measures the variability within a single sample. A higher standard deviation value indicates greater spread in the data. From the results are achieved in Table 6 it can be concluded that both the RHA and CP-admixture are

compatible with the 'Ashaka' Portland cement.

Table 6. Statistical Characteristics of OPC-RHA-CP Paste

Mix	Variable	Mean	SE Mean	StDev	Variance	CoefVar
RHA	Soundness	8.8	0.5	1.33	1.8	15,1
	Consistency	66.8	13.1	32.1	1030.2	48.0
	Initial Setting	174.7	58.7	58.7	3445.9	33.6
	Final Setting	276.7	80.9	80.9	6546.7	29.3
RHA-CP	Soundness	9.5	0.1	0.3	0.1	3.6
	Consistency	50.2	5.1	12.5	155.0	24.8
	Initial Setting	181.7	24.0	58.8	3457.1	32.4
	Final Setting	284.0	33.2	81.3	6612.4	28.6

Tables 7 and 8 are the linear regression model characteristics of the OPC-RHA-CP-admixture paste. The study on the experimental data used three regression models: (i) no-transformation, (ii) λ = 0.5 transformation, and (iii) box-cox transformation. The model characteristics are shown in the Tables 7 and 8, respectively, and the normality plot for the various mixes shown in Figure 7. All the models used seem to be adequate but the box-cox transformation shows more appropriateness compared with the no-transformation and λ = 0.5, based on the quality of the regression model characteristics achieved.

Table 7. Model Characteristics of OPC-RHA Paste

Parameter	RHA-CP-OPC Paste Characteristics		
	MODELI	MODEL II	MODEL III
Regression	*p = 0.040*	0.035	0.034
Soundness	*p = 0.550*	0.561	0.604
Initial Setting	*p = 0.773*	0.598	0.465
Final Setting	*p = 0.285*	0.225	0.192
Constant	*p = 0.678*	0.305	0.029
Model Summary	S (8.2782); R^2 (97.3 %)	*S* (0.4630); R^2 (97.7 %)	*S* (0.1128), R^2 (97.72 %),
Transformation	None	λ = 0.5	Box –Cox Rounded λ = 0 Estimated λ = 0.0235 95 % CI for λ = (-1.2430, 1.3850)
Regression Equation			

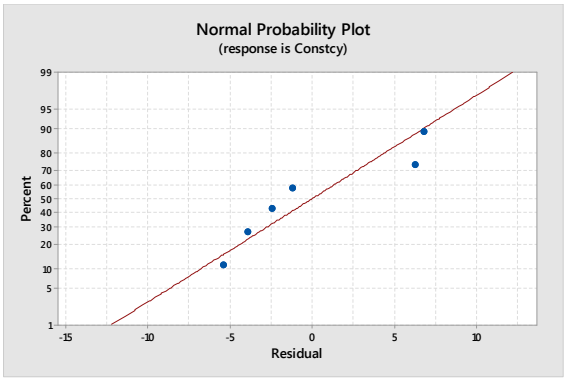

RHA-No Transformation

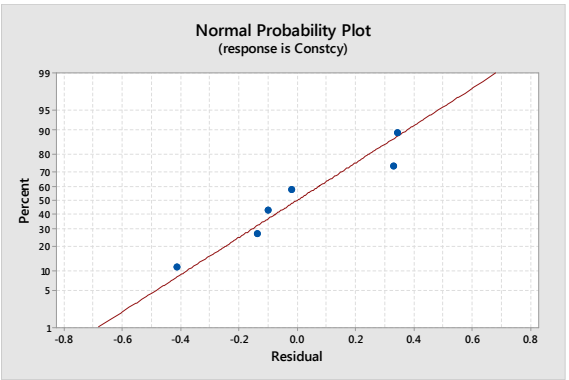

RHA: λ = 0.5

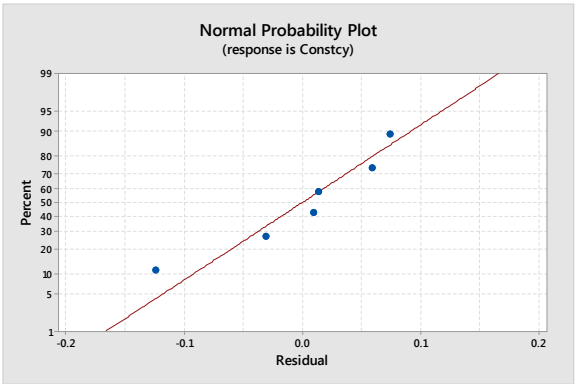

RHA: Box-Cox Transformation (Rounded λ = 0)

Table 8. Model Characteristics of OPC-RHA-CP Paste

Parameter	RHA-CP-OPC Paste Characteristics		
Regression	*p = 0.009*	0.007	0.004
Soundness	*p = 0.043*	0.031	0.014
Initial Setting	*p = 0.124*	0.103	0.067
Final Setting	*p = 0.362*	0.300	0.179
Constant	*p = 0.046*	0.305	0.029
Model Summary	S (1.5141); R^2 (99.4 %), $R^{2(pred)}$ (84.2 %)	*S* (0.0996); R^2 (99.5 %) $R^{2(pred)}$*(86.1%)*	*S* (0.1128), R^2 (97.72 %), $R^{2(pred)}$ (93.3%)
Transformation	None	λ = 0.5	Rounded λ = -1 (Box-Cox) Estimated λ = - 0.866784 95 % CI for λ = (-2.31928, 1.46672)
Regression Equation			

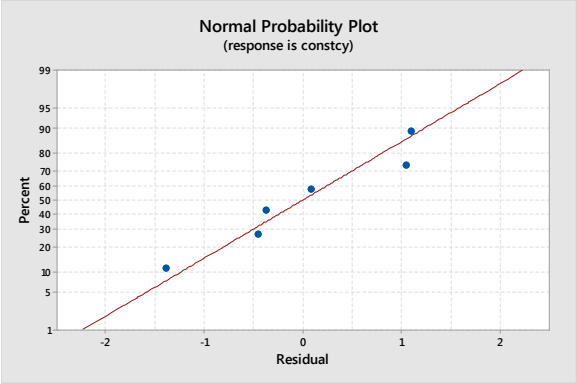

RHA-CP: No Transformation

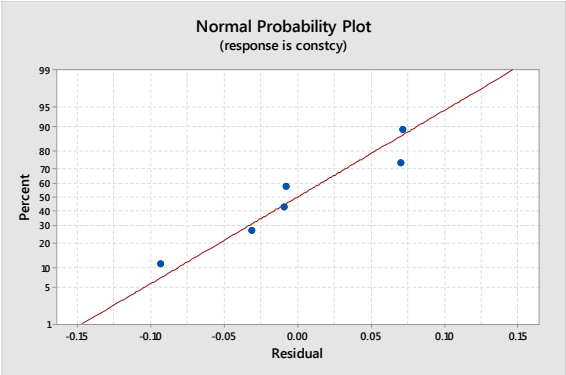

RHA-CP: $\lambda = 0.5$

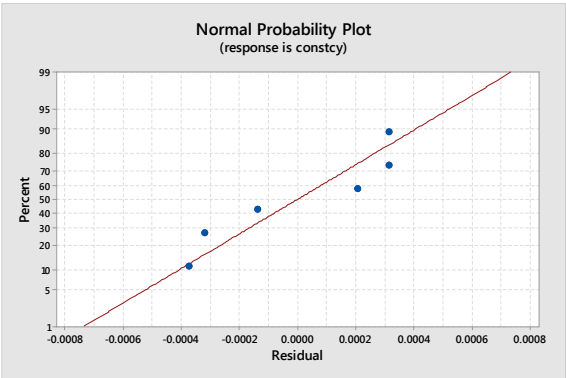

RHA-CP: Box-Cox Transformation (Rounded $\lambda = 0$)

Figure 7. Normality Plots for the Regression Models

5. Conclusions

An experimental investigation of the effects of using supplementary cement materials (SCM), in this case RHA, and an admixture, (Conplast SP 430) which is plasticizer, to evaluate the paste characteristics of mixes made with and without RHA, and CP-admixture as the case may be. The conclusions are:

i. RHA is pozzolanic and the limits of MgO and Na_2O are within the code's specifications. Using RHA, and/or RHA with CP-admixture will not cause unsoundness, and will not undergo any appreciable change after setting.

ii. A mixture of RHA alone will increase the water requirement because of the morphology of the RHA which encourages water absorption.

iii. Addition of CP-admixture to RHA mix will reduce the water affinity of RHA.

iv. The setting times will be affected by both the addition of RHA and CP-admixture which will allow adequate time for concreting before it sets.

Recommendation

The use of RHA with CP-admixture is recommended for good flow of the paste.

References

[1] Altine, J., Mamai, E.A., Bako, T., 2019. Rice waste conversion for economic empowerment in Taraba State, Nigeria: A review. IJTRD. 515-519.

[2] Abubakar, A.U., 2018. Progress on the use of rice husk ash (RHA) as a construction material in Nigeria. Sustainable Structure and Material. 1(2), 1-8.

[3] Darweesh, H.H.M., 2016. Black liquor waste as a cement admixture or cement and concrete admixtures. Biopolymers and Biotech Admixtures for Eco-Efficient Construction Materials. 99-130.

[4] Habeeb, G.A., Mahmud, H.B., 2010. Study on properties of rice husk ash and its use as cement replacement material, Materials Research. 13(2), 185-190.

[5] Dobiszewska, M., Beycioğlu, A. Investigating the influence of waste basalt powder on selected properties of cement paste and mortar. IOP Conf Materials Science and Engineering. 245.

[6] Samantasinghar, S., Singh, S.P., 2019. Fresh and hardened properties of fly ash-slag blended geopolymer paste and mortar. Int. J. Concr Struct Mater. 13, 47, 1-12.

[7] Conplast SP 430. Al Gurg FOSOOC LLC, Box 657, Duba, UAE.

[8] Elinwa, A.U., Mahmood, Y.A., 2002. Ash from timber waste as cement replacement material. Cement and Concrete Composites. 24(2), 219-222.

[9] Alkheder, S., Obaidat, Y.T., Taamneh, M., 2016. Effect of olive waste (Husk) on behavior of cement paste." Case Studies in Construction Materials. 5, 19-25.

[10] Mbugua, R., Salim, R., Ndambuki, J., 2016. Effect of Gum Arabic karroo as a Water-Reducing Admixture in Concrete. Materials. 9, 80, 1-16.

[11] Elinwa, A.U., 2016. Hospital ash waste-ordinary Portland cement concrete. Science Research. 4(3),

72-78.
[12] Elinwa, A.U., Abdulrazaq, A.A. Characteristics of polyvinyl chloride powder cement paste and concrete." Global Science Journal. 8(12), 377-388.
[13] BS EN 197, 2011. Cement Part 1: Composition, specifications and conformity criteria for common cements.
[14] ASTM C 618-12. Standard Specification for Coal Fly Ash and Raw or Calcined Natural Pozzolan for Use in Concrete.
[15] ASTM C 494-92. Standard Specification for Chemical Admixtures for Concrete.
[16] BS 4550-3.4, 1978. Methods of Testing Cement, Physical Tests-Strength Tests.
[17] BS 12: 1996. Specification for Portland Cement.

BILINGUAL PUBLISHING CO.
Pioneer of Global Academics Since 1984

Journal of Building Material Science
https://ojs.bilpublishing.com/index.php/jbms

ARTICLE

Comparative Analysis of Curing Methods: Natural and Activated Lateritic Concrete

Augustine Uchechukwu Elinwa*

Faculty of Engineering and Engineering Technology, Civil Engineering Department, Abubakar Tafawa Balewa University, PMB 0248, Bauchi, Bauchi State, Nigeria

ARTICLE INFO

Article history
Received: 23 February 2022
Accepted: 22 March 2022
Published Online: 07 April 2022

Keywords:
Standard and non-standard curing
Non-activated and activated laterite soil
Compressive strength
Linear shrinkage
Statistical and linear regression models

ABSTRACT

This work was on *non-activated* and *activated lateritic soil* used in proportions of 0% to 30%, to replace fine sand by wt. %, in the production of lateritic concrete. A mix of 1:2:4 was used, and the cube samples were cured in four (4) curing media of water, sand, polythene, and sawdust. The aim was to evaluate the effects of these curing methods on the mechanical strengths, and other properties of lateritic concrete. The sensitivity of the generated data was characterized statistically and developing linear regression models for predictions. For the Non-Activated Laterite soil (NALS, control mix (0%)), the design strength of 20 MPa was achieved by all the curing methods (standard and non-standard). However, for other replacement levels, water curing was adequate for 10% and 30%, sand at 10%, and sawdust for 20% and 30%, respectively. On the other hand, for the Activated Laterite soil (ALS), the 20 MPa design strength was met only at 0% replacement for all curing methods. Sawdust medium at 10% also satisfied the 20 MPa strength.

1. Introduction

Everything in life needs water for survival and is equally true for concrete and all construction works. Global water demand has been projected to increase by 55% in 2050. This is mainly from demands that related to growing urbanization in developing countries. It has also been postulated that the effect of this may cause cities to dig deeper to access water or depend on innovative solutions, or advanced technologies to meet their water demand [1].

The failures of concrete in many of our collapsed structures in Nigeria are due to improper curing. Curing of concrete works assists the hydration process of the cement, and the subsequent gain of adequate strength because of the formation of calcium silicate hydrates (CSH) that imparts strength to concrete. Curing therefore, maintains satisfactory moisture content, and temperature in concrete, for a period which immediately follows placing and finishing, so that

*Corresponding Author:
Augustine Uchechukwu Elinwa,
Faculty of Engineering and Engineering Technology, Civil Engineering Department, Abubakar Tafawa Balewa University, PMB 0248, Bauchi, Bauchi State, Nigeria;
Email: auelinwa@gmail.com

DOI: https://doi.org/10.30564/jbms.v4i1.4476

the desired properties may develop. This process has a strong influence on the properties of hardened concrete. Therefore, proper curing will increase properties such as durability, strength, water tightness, abrasion resistance, and volume stability. However, this problem of proper curing is aggravated by non availability of potable water or, when available, not suitable for curing as stipulated in the code of practice. Research values on water consumption from a study taken from 2012, and projected to 2050, showed that concrete production alone was responsible for 9% of global industrial water withdrawals in 2012. This was estimated to be 1.7% of the total consumption in 2050, which is approximately 75% of the water demand for concrete production and will likely occur in regions that are expected to experience water stress [2].

ASTM C31 [3] requires that standard cured cylinders for concrete acceptance should undergo initial curing between 60 °F (16 °C) and 80 °F (27 °C) for up to 48 hours after which they should be transferred to a moist room or water tank. It also defines two different curing conditions to be used for specific purposes. These are the standard curing and field curing.

The effects of non-standard curing on strength of concrete were undertaken by NRMCA [4], as a research project to study how the concrete strength was affected in different medium of curing. Two experiments to study this effect were mounted where test cylinders were exposed to exterior conditions in summer and winter months and compared these results to standard cured specimens. In both cases, concrete cylinders were prepared from a mixture with cement content of 475 lbs./yd^3 (282 kg/m^3), and fly ash content of 50 lbs./yd^3 (30 kg/m^3), at a water-cementitious materials (w/cm) ratio of 0.52, and cured for the periods of 3, 7, 28, and 90 days. Four methods of curing were adopted: standard curing, lab-air-dry, outside for 48 hours, moist cured, and outside until time of test. The results of the test are shown in Table 1. Details of the conclusions are contained the work [4].

Nahata et al. [5] worked on the effect of curing methods on cement mortar that were cured for 28 days. He used the findings from the literature review and experimental works carried out as per ASTM standards to evaluate compressive strength of mortar cubes. They used different curing compounds, and a mix ratio of 1:2.75, and water/binder ratio of 0.45 to 0.60, and concluded that using membrane curing compounds achieved an efficiency of 80% – 90% as compared to conventional curing.

Rahman et al. [6] researched on the effect of curing methods on compressive strength of concrete using a concrete mix of 1:2:4, with four different curing methods, dry-air, complete immersion in water, wrapped with gunny bags, and sprinkling with water. They cured the specimens for 7, 14, 21 and 28 days, and concluded that the specimens wrapped with gunny bags gave the highest strength after 28 days of curing.

Table 1. Compressive Strength

Weather Exposure	Age (Days)	Control Strength (Psi/MPa))	Percent of Control Strength at Same Age (%)		
			Lab-air-dry	Out 48h, moist)	Outside
Cold weather Series D 335	1	1508 (10.1)			
	3	2828 (18.9)		46	14
	7	3852 (25.8)	95	68	40
	28	745 (5.0)	88	78	66
	90	5374 (36)	74	90	82
Hot Weather Series D 338	1	784 (5.3)		180	180
	3	2370 (15.9)		89	86
	7	3176 (19.1)		81	90
	28	4384 (9.3)		78	84
	90	5659 (37.9)		84	80

Paulik used five (5) curing methods for works on a bridge construction to arrive at the best strength for the work. The curing methods he adopted and the achieved strengths are shown in Tables 2 and 3. He observed that the differences in compressive strengths at early ages were almost 300% after 48 hours when the specimens cured at 2 °C in air were compared with specimens cured at 20 °C in water. However, these differences gradually diminished after 28 days [7].

Table 2. Curing regimes of the specimens [7]

Group	Curing Conditions	Number of Specimens
Series A	Cured in water at 20 °C (± 1 °C)	9
Series B	Sealed and cured at 20 °C (± 1 °C)	9
Series C	Cured on air at 20 °C (± 1 °C)	9
Series D	Cured on air at 2 °C (± 2 °C) covered	9
Series E	Cured on air at 2 °C (± 2 °C) uncovered	9

Gayarre et al. [8] studied the effect of different curing conditions on the compressive strength of recycled aggregates with water-cement ratio of 0.65, and replacement levels of 0%, 20%, 50%, and 100%, to replace the coarse aggregate. The specimens were cured (standard curing and open-air curing), for 28 days. They concluded that 28 days compressive strengths of both recycled and natural aggregates were almost the same when standard curing environment was considered but differs by 20% when cured in open-air conditions.

The influence of non-standard curing practice on the strengths of specimens and in-situ concrete was evaluated by Arafah et al. [9], using experimental testing methods. They collected samples from construction sites distributed over two areas of distinct climate conditions described as hot and dry (arid), and hot and moist (coastal climates), and tested using cores taken from slab, beam, and column elements. Curing was by water sprinkling twice a day for 7 days with or without burlap cover. They concluded that curing by water sprinkling twice a day and with or without burlap cover was far below the ACI-318 requirements.

Table 3. Compressive strength and density of the specimens after 2, 7, and 28 days [7]

Group	2 days		7 days		28 days	
	Density (g/dm^3)	Strength (N/mm^2)	Density (g/dm^3)	Strength (N/mm^2)	Density (g/dm^3)	Strength (N/mm^2)
Series A	2344	41.8	2358	63.4	2339	81.5
Series B	2337	41.0	2355	58.3	2332	71.8
Series C	2328	39.2	2316	61.4	2317	68.4
Series D	2300	16.1	2344	45.2	2348	66.1
Series E	2308	13.4	2318	40.5	2362	67.3

Udoeyo et al. [10] used thirty mixes of differing water-binder ratio containing 0%, 10%, 20%, 30%, 40%, and 50% laterite as partial replacements for sand to prepare laterized concrete specimens used to study the effect of non-standard curing methods on the strength of specimen. The results showed that with continuous wetting of the non-standard curing media by sprinkling with water, the strength of concrete obtained was comparable to those cured using the control method. They also opined that the strength of the sand- and sawdust-cured specimen was in some instances the same as or higher than those of the standard cured specimens at an early age (7 days).

The thrust of the present investigation is anchored on the fact that in some parts of Nigeria, water for proper curing for construction works at times becomes difficult for many reasons. Some of these reasons are desertification and arid nature of the environment in the northern part of the country, and some parts in the eastern parts of the country where the water is salty [11]. Therefore, it becomes imperative to explore other methods of curing that would otherwise achieve the desired strength and other impacting properties of the concrete materials. This will add to the existing knowledge on curing methods and their effects on strength development in the area of research, which is lateritic concrete. In furtherance of research works in this area, the importance of documented data on different methods of curing become very important. In this study, four curing methods water, sand, polythene and sawdust, are used to assess the compressive strengths of lateritic soil concrete using experimental methods. The laterite soil was used in proportions of 0%, 10%, 20% and 30% by wt. % of cement to replace part of the sand and cured for 28 days.

2. Material

The materials used for this investigation are Ashaka Portland cement, fine and coarse aggregates, lateritic soil, and potable water for mixing. Table 4 shows the physical properties of both the cement, lateritic soil, and the aggregates, while Table 5 is the chemical properties of the cement and lateritic soils (Normal and Activated). The activated lateritic soil was activated to an elevated temperature between 400 ^oC and 600 ^oC in a kiln and cooled for 2 hours. The sieve analyses of the lateritic soil, and aggregates are shown in Table 6. The soil material retained by sieve size 150 μm, was used for the investigation.

Table 4. Physical Properties of the Aggregates and Lateritic Soil

Type	Lateritic Soil	Aggregate	
		Fine	Coarse
Specific gravity	2.52	2.61	2.7
Impact value (%)	-	-	7.1
Crushing value (%)	-	-	22.6
Bulk density (kg/m^3)	1507	1501.5	1612.5

Table 5. Chemical Characteristics of Natural and Activated Lateritic Soil

Compound	Ashaka Cement	Lateritic Type	
		Natural [5]	Activated
	Weight (%)	Weight (%)	Weight (%)
Fe_2O_3	2.90	2.38	6.80
TiO_2	-	0.82	0.82
K_2O	0.21	0.13	0.03
SiO_2	19.90	77.80	46.80
MgO	1.50	0.13	0.13
Al_2O_3	5.60	18.40	28.90
P_2O_5	-	0.10	0.30
CrO_3	-	0.09	0.09
SO_3	2.30	0.09	0.09
CaO	63.70	0.04	2.40
ZrO_2	-	0.03	1.40
MnO	-	0.01	0.97
ZnO	-	0.01	0.41
Na_2O	0.21	-	-

Table 6. Sieve Analysis of Natural and Activated Lateritic Soil

Sieve size	Fine Aggregate (%)		Lateritic Soil (%) [5]	
	Retained	Passing	Retained	Passing
5.00	0.00	100	-	-
2.63	10.73	89.27	-	-
2.00	3.37	85.54	-	-
1.18	17.23	68.31	1.90	98.10
600 µm	33.00	35.31	27.20	70.90
425 µm	-	-	18.00	52.90
300 µm	21.03	14.28	25.30	27.60
212 µm	-	-	11.70	15.90
150 µm	12.13	2.15	12.40	3.50
75 µm	-	-	3.50	0.00
63 µm	1.48	0.67	-	-
Pan	0.67	0		0.00

3. Experimental Procedure

The mix proportion used for this work is approximately a mix of 1:2:4, with a cement content of 318 kg/m^3, fine and coarse aggregate contents of 673 kg/m^3 and 1234 kg/m^3 respectively, and water content of 175 kg/m^3. The mix was designed for a concrete strength of 20 MPa at 28 days of curing. The work used two types of lateritic soils. One was in its natural state, and the second was activated to a temperature of 400 °C to 600 °C. Four mixes each were used for both the natural and activated soils at replacement levels of 0%, 10%, 20% and 30%, of the sand by wt. %. The mix with 0% replacement is labeled M-00, as the control mix. The rest of the mixes had attached to them suffices reflecting their different levels of replacement. Curing of the specimens was achieved using different media: water, sand, sawdust and polythene. The curing methods adopted for the sand, sawdust, and polythene were the same as used by Udoeyo et al. [10]. Details of these methods are found in their works. The specimens were cured for 3, 7, 14 and 28 days, before testing to failure.

Slump and compressive strength of lateritic concrete

The work was mostly on the compressive strength, and a total of one hundred and sixty (160) cube specimens of dimensions 150 mm were cast and cured as stated earlier. Eighty (80) each were cast for the natural and activated soils. At the end of each curing regimes, three of the cube specimens were tested to failure using an ELE compression machine, and the average recorded. The slump and cube compressive strength are shown in Tables 7 and 8 respectively.

Table 7. Slump of Normal and Activated Lateritic Soil Concrete

Soil Type	M-00	M-10	M-20	M-30
Slump–Normal (mm)	20	30	30	30
Slump-Activated (mm)	35	30	18	13

Table 8. Cube Compressive Strength of Normal and Activated Lateritic Soil Concrete

Material Type	Mix No	Curing Medium	Compressive Strength (MPa)			
			3 d	7 d	14 d	28 d
Lateritic soil	M-00	Water	14.8	18.1	20.1	22.9
	M-10		11.3	10.2	13.8	19.9
	M-20		8.0	15.2	16.4	18.9
	M-30		13.5	13.9	15.9	20.8
	M-00	Sand	13.0	13.8	19.0	22.2
	M-10		10.1	14.1	16.5	21.0
	M-20		10.3	17.7	15.1	18.1
	M-30		17.0	17.3	17.6	18.1
	M-00	Polythene	6.9	14.6	13.1	20.2
	M-10		14.0	13.1	15.2	17.5
	M-20		10.9	14.9	13.9	16.2
	M-30		12.4	16.5	16.9	17.9
	M-00	Sawdust	18.1	17.6	18.0	22.6
	M-10		12.0	13.8	15.9	17.7
	M-20		13.7	15.4	17.0	20.1
	M-30		12.4	12.6	20.3	22.2
Activated lateritic soil	M-00	Water	18.1	14.8	19.9	24.3
	M-10		11.8	14.8	19.9	17.8
	M-20		12.1	11.6	11.2	12.2
	M-30		8.5	12.1	12.6	13.1
	M-40		9.7	13.1	12.8	15.8
	M-00	Sand	13.4	13.3	18.9	23.1
	M-10		10.6	15.3	15.0	17.8
	M-20		7.4	7.9	13.0	13.1
	M-30		8.7	8.7	11.9	13.3
	M-40		9.3	8.9	12.9	10.9
	M-00	Polythene	11.6	17.6	17.9	25.5
	M-10		11.3	14.5	15.4	14.5
	M-20		8.0	9.0	11.6	12.9
	M-30		8.3	9.2	11.4	11.6
	M-40		9.3	10.0	11.7	13.6
	M-00	Sawdust	14.6	6.9	13.0	20.0
	M-10		10.7	14.1	15.5	21.8
	M-20		9.1	6.4	10.4	11.0
	M-30		9.4	8.9	11.4	10.9
	M-40		9.8	10.2	12.0	11.2

4. Discussion

(i) Characteristics of the natural and activated lateritic soil

From Table 5 the characteristics of the NLS and ALS showed that the totals of $SiO_2 + Fe_2O_3 + Al_2O_3$ are approximately 99% and 83% respectively. These are well above the levels stipulated by ASTM for pozzolanic activity. Therefore, in both conditions the NLS and ALS are pozzolanic and can only go into chemical reaction in the presence of lime and water. The CaO contents are 0.04 and 2.40 respectively, showing they have no cementing values. The Fe_2O_3 and Al_2O_3 in NLS are 35% and 64% of the ALS, while the SiO_2 in the ALS is 60% of the NLS.

(ii) Basic characteristics of the lateritic concrete

The statistical Equations (i) - (vi), contained in Minitab 17 Software package were used to derive the values of the Mean, Standard Error of Mean *(SEMean)*, Standard Deviation (*StDev)*, Variance, Coefficient of Variation *(CoefVar)*, and Range (Maximum – Minimum), of both natural and activated lateritic soil are shown below:

$$\bar{x} = \frac{\sum x_i}{n} \quad (i)$$

$$\sigma_M = \frac{\sigma}{\sqrt{n}} \quad (ii)$$

$$\sigma^2 = \frac{\sum (x_i - \bar{x})^2}{n} \quad (iii)$$

$$\sigma = \sqrt{\frac{\sum (x_i - \bar{\bar{x}})^2}{n}} \quad (iv)$$

$$CV = \frac{\sigma}{\bar{x}} \quad (v)$$

$$R = (Max.value - Min.value) \quad (vi)$$

Where:

$\bar{x}$ = Population means

x_i = Sum of all the population observations

n = Number of population observation

σ = Standard deviation of the population

σ^2 = Variance

σ_M = Standard error of Mean

R = Range of the population observation

The values obtained are shown in Tables 8 and 9 respectively. Table 8 shows the within test results data on the basic characteristics of lateritic soil concrete (Normal and Activated). The within-test is the variation that occurred in the lateritic-cement matrix as curing proceeded within the same mix. Thus, this was for a particular mix measured along the row as curing proceeded. Table 9 is the batch-to-batch data results and is the test results taken down the column. This involved different mixes which are measured at the same age as curing proceeded.

The mean value characterizes the central tendency or location of the data, and the coefficient of variation provid es a general feeling about the performance of a method and its distribution around the mean. It expresses the variation as a percentage of the mean. Thus, the larger the coefficient of variation is, the greater is the spread in the data. These behaviors are reflected in the values obtained in Tables 9 and 10.

The standard error of the mean *(SE Mean*) estimates the variability between sample means, and the standard deviation and thus, establishes a benchmark for estimating the overall variation of a process. Whereas the standard error of the mean estimates the variability between samples, the standard deviation measures the variability within a single sample. The variance (standard deviation squared) measures how spread-out the data are about their mean. A higher standard deviation value indicates greater spread in the data. The greater the variance is the greater the spread in the data. The general observation made on the data as they affect both the mix and age is that the statistical values decreased as the replacement levels

(iii) Basic Characteristics of the Lateritic –Concrete

Table 9. Basic Statistics for Within-Test for Lateritic-Concrete.

Type	Medium	Age (Days)	Mean	SE Mean	StDev	Var	CoefVar	Min	Max	Range
Normal	Water	3	11.90	1.49	2.97	8.85	24.99	8.00	14.80	6.80
		7	14.35	1.64	3.28	10.74	22.83	10.20	18.10	7.90
		14	16.55	1.31	2.62	6.87	15.84	13.80	20.10	6.30
		28	20.63	0.85	1.70	2.90	8.26	18.90	22.90	4.00
Activated		3	12.04	1.66	3.70	13.70	30.74	8.50	18.10	9.60
		7	13.58	0.77	1.54	2.38	11.35	11.60	14.80	3.20
		14	15.28	1.91	4.26	18.17	27.89	11.20	19.90	8.70
		28	16.64	2.16	4.82	23.24	28.97	12.20	24.30	12.10
Normal	Sand	3	12.60	1.61	3.22	10.35	25.54	10.10	17.00	6.90
		7	15.72	1.03	2.06	4.24	13.10	13.80	17.70	3.90
		14	17.05	0.83	1.65	2.74	9.70	15.10	19.00	3.90
		28	19.85	1.04	2.08	4.32	10.47	18.10	22.20	4.10
Activated		3	9.88	1.02	2.28	5.20	23.07	7.40	13.40	6.00
		7	10.82	1.47	3.28	10.73	30.28	7.90	15.30	7.40
		14	14.34	1.25	2.79	7.76	19.43	11.90	18.90	7.00
		28	15.64	2.18	4.87	23.68	31.11	10.90	23.10	12.20

Table 9 continued

Type	Medium	Age (Days)	Mean	SE Mean	StDev	Var	CoefVar	Min	Max	Range
Normal	Sawdust	3	12.43	0.46	0.91	0.83	7.33	11.60	13.70	2.10
		7	14.85	1.08	2.16	4.68	14.56	12.60	17.60	5.00
		14	17.80	0.94	1.87	3.51	10.53	15.90	20.30	4.40
		28	20.65	1.13	2.25	5.07	10.90	17.70	22.60	4.90
Activated		3	10.72	1.01	2.25	5.07	21.00	9.10	14.60	5.50
		7	9.30	1.38	3.09	9.54	33.22	6.40	14.10	7.70
		14	11.66	0.42	0.95	0.90	8.13	10.40	13.00	2.60
		28	14.98	2.43	5.44	29.62	36.33	10.90	21.80	10.90
Normal	Polythene	3	11.05	1.52	3.04	9.26	27.53	6.90	14.00	7.10
		7	14.78	0.70	1.39	1.94	9.43	13.10	16.50	3.40
		14	14.78	0.83	1.66	2.76	11.24	13.10	16.90	3.80
		28	17.95	0.83	1.67	2.78	9.28	16.20	20.20	4.00
Activated		3	10.72	1.01	2.25	5.07	21.00	9.10	14.60	5.50
		7	9.30	1.38	3.09	9.54	33.22	6.40	14.10	7.70
		14	11.66	0.42	0.95	0.90	8.13	10.40	13.00	2.60
		28	14.98	2.43	5.44	29.62	36.33	10.90	21.80	10.90

Table 10. Basic Statistics for Batch-to-Batch-Test for Lateritic-Concrete

Type	Medium	Mix No	Mean	SE Mean	StDev	Variance	CoefVar	Minimum	Maximum	Range
Normal	Water	M-00	18.98	1.70	3.41	11.62	17.97	14.80	22.90	8.10
		M-10	13.80	2.17	4.34	18.81	31.43	10.20	19.90	9.70
		M-20	14.62	2.34	4.68	21.88	31.99	8.00	18.90	10.90
		M-30	16.02	1.68	3.35	11.24	20.92	13.50	20.80	7.30
Activated		M-00	19.28	1.98	3.96	15.68	20.55	14.80	24.30	9.50
		M-10	16.07	1.77	3.54	12.50	22.00	11.80	19.90	8,10
		M-20	11.85	0.23	0.45	0.20	3.81	11.20	12.20	1.00
		M-30	11.58	1.05	2.09	4.37	18.06	8.50	13.10	4.60
		M-40	12.85	1.25	2.50	6.23	19.42	9.70	15.80	6,10
Normal	Sand	M-00	12.60	1.61	3.22	10.35	25.54	10.10	17.00	6.90
		M-10	15.72	1.03	2.06	4.24	13.10	13.80	17.70	3.90
		M-20	17.05	0.83	1.65	2.74	9.70	15.10	19.00	3.90
		M-30	19.85	1.04	2.08	4.32	10.47	18.10	22.20	4.10
Activated		M-00	17.18	2.37	4.74	22.45	27.59	13.30	23.10	9.80
		M-10	14.68	1.50	2.99	8.96	20.39	10.60	17.80	7.20
		M-20	10.35	1.56	3.12	9.76	30.19	7.40	13.10	5.70
		M-30	10.65	1.16	2.32	5.40	21.81	8.70	13.30	4.60
		M-40	10.50	0.91	1.82	3.31	17.32	8.90	12.90	4.00
Normal	Sawdust	M-00	12.43	0.46	0.91	0.83	7.33	11.60	13.70	2.10
		M-10	14.85	1.08	2.16	4.68	14.56	12.60	17.60	5.00
		M-20	17.80	0.94	1.87	3.51	10.53	15.90	20.30	4.40
		M-30	20.65	1.13	2.25	5.07	10.90	17.70	22.60	4.90
Activated		M-00	13.63	2.70	5.39	29.07	39.57	6.90	20.00	13.10
		M-10	14.52	2.53	5.06	25.63	34.85	10.70	21.80	11.10
		M-20	9.22	1.02	2.04	4.18	22.15	6.40	11.00	4.60
		M-30	10.15	0.60	1.19	1.42	11.73	8.90	11.40	2.50
		M-40	10.80	0.50	0.99	0.99	9.20	9.80	12.00	2,20
Normal	Polythene	M-00	11.05	1.52	3.04	9.26	27.53	6.90	14.00	7.10
		M-10	14.78	0.70	1.29	1.94	9.43	13.10	16.50	3.40
		M-20	14.78	0.83	1.66	2.76	11.24	13.10	16.90	3.80
		M-30	17.95	0.83	1.67	2..78	9.28	16.20	20.20	4.00
Activated		M-00	18.15	2..85	5.69	32.43	31.38	11.60	25,50	13.90
		M-10	13.93	0.90	1.80	3.24	12.93	11.30	15.40	4.10
		M-20	10.38	1.13	2.27	5,14	21.84	8.00	12.90	4.90
		M-30	10.13	0.82	1.63	2.66	16.12	8.30	11.60	3.30
		M-40	11.15	0.96	1.92	3.68	17.21	9.30	13.60	4.30

increased and increased as the age of the lateritic concrete increased. The assertion therefore is that in developing the model equations consideration of the material effect is important, and should be integrated into the equation.

(iv) Slump and Compressive Strength

The slump is used to measure the workability or consistency of fresh concrete mix. The slump of the lateritic soil concrete in its natural state improved the workability as the replacement of sand by lateritic soil increased. The reverse was the case when the lateritic soil was activated to a higher temperature. This behavior is more pronounced on the development of the compressive strength.

Figure 1 (a-c) gives a general idea on the development of lateritic concrete strength for natural and activated lateritic concrete. The differences in the strength developments and their classifications are shown in Table 11. Curing with water, sand, and polythene improved both the compressive strengths of NLS and ALS. The increase in compressive strengths were approximately 6%, 4% and 26%, respectively. Although, sawdust curing medium registered a decrease for ALT as compared to NLS, it still met the concrete designed strength of 20 MPa. The increase recorded for the polythene curing medium was remarkable and thus recommended as curing medium when both NLS and ALS without any additives are considered. At 10% sawdust replacement by wt. % of sand, curing with water and sand marginally achieved the 20 MPa design strength. This design strength was also achieved for ALS specimens cured with sawdust (21.8 MPa). For other replacements, 20% and 30%, the design strength was achieved for specimens cured with sawdust (20.1 MPa), at 20% replacement, and specimens cured in water (20.8 MPa) and sawdust (22.2 MPa), at 30% replacement. However, they were only for NLS specimens. The conventional 7/28th day strength for specimens cured in water (NLS and ALS) are 79% and 61%, respectively. However, for other mixes, where sawdust was used in various proportions to replace sand by wt. % of sand are 66% (average for NLS), and 91%. For mixes containing proportions of laterite soil by wt. % of sand (average of 10%, 20%, and 30%), the 7/28th day strength (Normal and activated), are 66% and 91% (average for ALS), respectively. The high value recorded for the activated laterite soil-concrete were due to the low strength recorded.

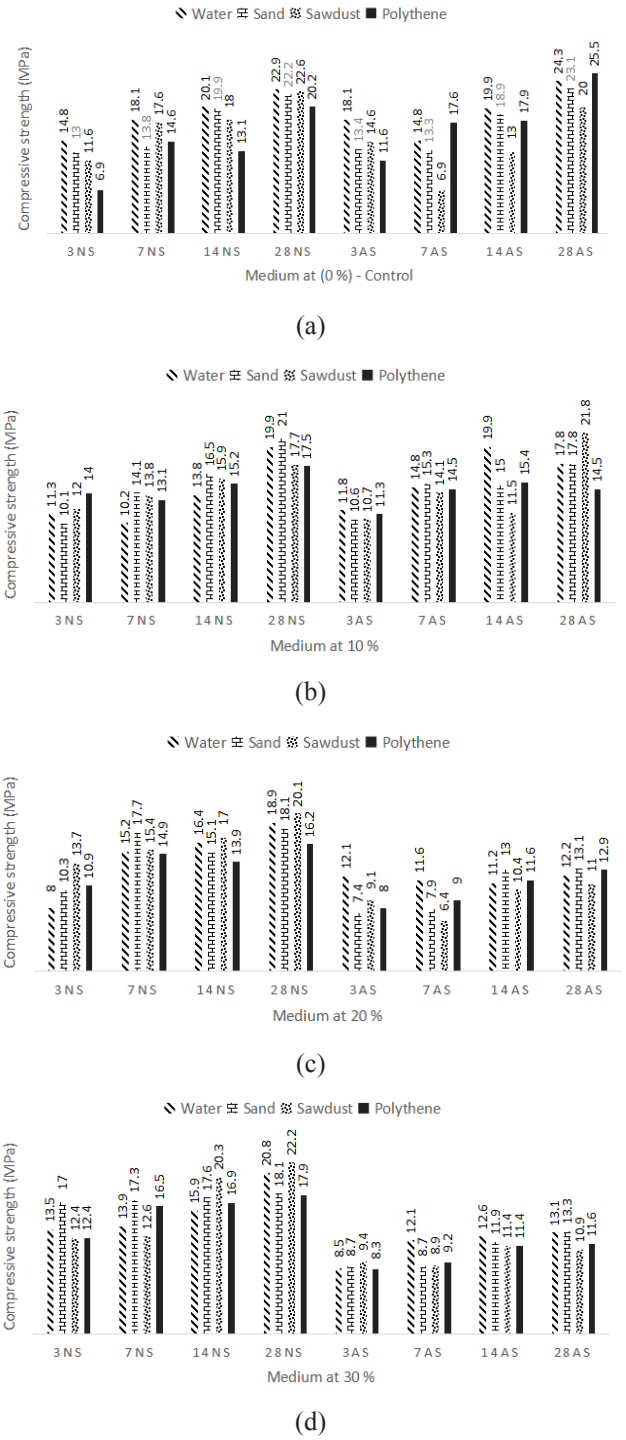

Figure 1. Compressive Strength of Lateritic Concrete in Different Medium of Curing

Table 12 is a classification table for the concrete grades, based on the compressive strengths achieved by the different curing methods, and how they met the strength of 20 MPa as the design strength. It showed that the specimens without sawdust (control) cured in standard and non-standard medium, met the 20 MPa design strength for both the NLS and ALS-concrete. However, it

was observed that the ALS cured with sawdust reduced in strength by approximately 12% when compared with NLS (Table 11). It therefore showed that at 0% replacement the standard and non-standard methods gave a normal reinforced concrete grade of 19.9 MPa – 24.3 MPa. The lateritic concrete strengths (normal and activated) at 10%, 20%, and 30% replacements respectively, fell below the design strength of 20 MPa, and therefore could be used for other grades of concretes (Table 12). These are designated as lateritic-concrete lintels strength (14.5 MPa to 18.9 MPa) and blinding lateritic-concrete (10.9 MPa to 13.3 MPa).

Table 11. Compressive Strength of Lateritic Concrete: Comparison in Different Curing Medium

Repl (%)	Medium	Lateritic Concrete			
		Non-activated	Activated	Diff. (MPa)	Diff (%)
0	Water	22.9	24.3	+1.4	+6.1
	Sand	22.2	23.1	+0.9	+4.1
	Polythene	20.2	25.5	+5.3	+26.2
	Sawdust	22.6	20.0	–2.6	–11.5
10	Water	19.9	17.8	–2.1	–10.6
	Sand	21.0	17.8	–3.2	–15.2
	Polythene	17.5	14.5	–3.0	–17.1
	Sawdust	17.7	21.8	+4.1	+23.2
20	Water	18.9	12.2	–6.7	–35.4
	Sand	18.1	13.1	–5.0	–27.6
	Polythene	16.2	12.9	–3.3	–20.4
	Sawdust	20.1	11.0	–9.1	–45.3
30	Water	20.8	13.1	–7.7	–37.0
	Sand	18.1	13.3	–4.8	–26.5
	Polythene	17.9	11.6	–6.3	–35.2
	Sawdust	22.2	10.9	–11.3	–50.9

Table 12. Classification of Strength Levels

Strength level (MPa)	Mix (%)	Curing Medium	Soil texture	Application
19.9 - 24.3	0	Polythene, Water, Sawdust, Sand	Normal, Activated	Slab Beam Column
	10			
	10	Water, Sand	Normal	
	20	Sawdust	Activated	
	30	Sawdust	Normal	
	30	Water Sawdust	Normal	
14.5 – 18.9	10	Polythene	Normal	Lintel
	10	Sawdust	Normal	
	10	Water	Activated	
	10	Sand	Activated	
10.9 – 13.3	20 & 30	Water Sand Sawdust Polythene	Activated	Blinding

(vi) Linear Regression Analysis of Lateritic Concrete

The statistical analysis was carried out on the compressive strength of lateritic concrete (NLS and ALS), using the Minitab 19 Statistical Software, on the conventional and non-standard methods of curing. The relevant linear regression equations in the study are from Equations (vii) to (ix).

$$Y = \beta_0 + \beta_1 x + \varepsilon \quad (vii)$$

Where

ε = the random error

β_0 = least square estimates of the intercept

β_1 = slope of model

$$\widehat{\beta}_0 = \bar{y} - \widehat{\beta}_1 \bar{x} \quad (viii)$$

$$\widehat{\beta}_1 = \frac{\sum_{i1}^{n} y_i x_i - \frac{\left(\sum_i^n y_i\right)\left(\sum_1^n x_i\right)}{n}}{\sum_1^n x_i^2 - \frac{\left(\sum_1^n x_i\right)^2}{n}} \quad (ix)$$

Where

$$\bar{y} = \left(\frac{1}{n}\right) \sum_1^n y_i \text{ , and } \bar{x} = \left(\frac{1}{n}\right) \sum_1^n x_i \,. \quad (x)$$

The two (2) factors considered were the percentage lateritic soil content (Mix), and the Age of the lateritic concrete samples (curing). Table 13 showed the linear regression models obtained for the different conditions of the lateritic soil, mix, and methods of curing the specimens. The linear regression models for the lateritic concrete (NLS and ALS), can be generally represented by: $f_c = A \mp Bx + Cx_1$,

Where

f_c = the compressive strength of the lateritic concrete (NLS and ALS),

A, x, and $x1$, are constant, mix, and age, respectively, of the lateritic concrete.

The analysis of variance (ANOVA) showed that the regression models, mix and age, are significant with p-values < 0.005, except for NLC mixes for non-standard method of curing (sand, polythene, and sawdust). The other characteristics of these models are also shown in the table. The standard deviations of the samples vary from 2.449 to 3.478. The interactions between the mix and age

Table 13. Linear Regression Data for Lateritic Concrete

Curing Medium	LatConc Type	Stat. Term	Coef	St.Coef	T-Value	P-Value	Signif	St.Dev	R^2 (%)
Water	NLC	Const	10.99	1.43	7.66	0.000	Significant	3.018	55.35
		Mix	-0.879	0.39	-2.26	0.029	Significant		
		Age	2.796	0.39	7.17	0.000	Significant		
	ALC	Const	18.48	1.44	12.83	0.000	Significant	3.032	58.52
		Mix	–2.874	0.392	–7.34	0.000	Significant		
		Age	1.287	0.392	3.28	0.002	Significant		
Sand	NLC	Const	10.27	1.16	8.82	0.000	Significant	2.449	54.95
		Mix	0.072	0.32	0.23	0.822	NSignificant		
		Age	2.340	0.32	7.40	0.000	Significant		
	ALC	Const	13.44	1.13	11.90	0.000	Significant	2.378	72.63
		Mix	–2.439	0.307	–7.94	0.000	Significant		
		Age	2.367	0.307	7.70	0.000	Significant		
Polythene	NLC	Const	8.23	1.19	6.91	0.000	Significant	2.507	49.61
		Mix	0.469	0.324	1.45	0.154	NSignificant		
		Age	2.091	0.324	6.46	0.000	Significant		
	ALC	Const	11.79	1.38	8.55	0.000	Significant	2.902	40.62
		Mix	–1.449	0.375	–3.87	0.000	Significant		
		Age	1.527	0.375	4.07	0.000	Significant		
Sawdust	NLC	Const	9.52	1.30	7.34	0.000	Significant	2.728	57.02
		Mix	–0.022	0.352	–0.06	0.950	NSignificant		
		Age	2.722	0.352	7.72	0.000	Significant		
	ALC	Const	14.85	1.65	8.98	0.000	Significant	3.478	60.08
		Mix	–2.99	0.449	–6.67	0.000	Significant		
		Age	2.24	0.449	4.99	0.000	Significant		

of the lateritic concrete, ranged from 49.61% to 72.63%, and the residual plots models showed that there were few residuals [12], and hence apparent limited outliers [13].

5. Conclusions

The effect of curing methods used in the evaluation of the compressive strength, and other characteristics of NALS and ALS have been studied. The conclusions on the findings are that, the material properties of the lateritic soils are important in considering model developments and their performances for lateritic soils. The slumps of the NALS and ALS, the statistical characteristics of the data, and the values of the compressive strengths achieved on the work, testify to the fact of the importance of the material characteristics in the performance of lateritic soils for engineering purposes.

The work also showed that the various methods of curing studied assisted in the classifications of grades of NALS and ALS-concrete. The four (4) methods of curing adopted (water, sand, polythene, and sawdust), for this work are suitable both for NALC and ALS-concrete. However, when SDA was used to replace part of the sand by wt. %, the curing medium can become sensitive to the state in which the laterite soil is in, either in the normal or activated state. This becomes a determining factor for strength classification.

Conflict of Interest

Author declares that there is no conflict of interest.

References

[1] OECD, 2012a. OECD Environmental Outlook to 2050: The Consequences of Inaction, OECD Publishing Paris.

[2] Miller, S.A., Horvath, A., Monteiro, P.J.M., 2018. Impacts of booming concrete production on water resources worldwide. Nature Sustainability. 1, 69-76.

[3] ASTM C31/C31M-21. Standard Practice for Making and Curing Concrete Test Specimen in the Field.

[4] Obia, K., Rodriguez, F., Ben-Barka, S., 2005. Effects of non-standard curing on strength of concrete. NRMCA Research Laboratory – Series D335 and D338, 1-4.

[5] Nahata, Y., Kholia, N., Tank, T.G., 2014. Effect of

curing methods on efficiency of curing of cement mortar. APCBEE Procedia. 9, 222-229.

[6] Rahman, M.S., Islam, S.M.M., Abedin, M.Z., 2012. Effect of curing methods on compressive strength of concrete. Bangladesh Journal of Agricultural Engineering. 23(1 & 2), 71-76.

[7] Paulik, P., 2013. The effect of curing conditions (In-situ vs. Laboratory) on compressive strength development of high strength concrete. Procedia Engineering. 65, 113-119.

[8] Gayarr, F.L., Pérez, C.L., Serrano, M.A., 2014. The effect of curing conditions on the compressive strength of recycled aggregate concrete. Construction and Building Materials. 53, 260-266.

[9] Arafah, A., Al-Zaid, R., Haddad, M.Al., 1996. Influence of non-standard curing on the strength of concrete in arid areas. Cement and Concrete Research. 26(9), 1341-1350.

[10] Udoeyo, F., Brooks, R., Utam, C., et al., 2010. Effect of non-standard curing methods on the compressive strength of laterized concrete. APRN Journal of Engineering and Applied Sciences. 5(2), 6-20.

[11] Mbadike, E.M., Elinwa, A.U., 2011. Effect of salt water in the production of concrete. African Journals Online (AJOL). 30(2), 105-110.

[12] Field, A., 2002. Discovering Statistics Using SPSS for Windows Sage Publications, London. pp. 492.

[13] Razak, H.A., Wong, H.S., 2004. Strength estimation model for high-strength concrete incorporating metakaolin and silica fume. Cement and Concrete Research. 35, 688-695.

BILINGUAL PUBLISHING CO.
Pioneer of Global Academics Since 1984

Journal of Building Material Science
https://ojs.bilpublishing.com/index.php/jbms

ARTICLE

Analysis of Heat Transfer Phenomena inside Concrete Hollow Blocks

Joelle Al Fakhoury[1,2] Emilio Sassine[1*] Yassine Cherif[2] Joseph Dgheim[1] Emmanuel Antczak[2] Thierry Chartier[2]

1. Lebanese University, Habitat and Energy Unit, Group of Mechanical, Thermal and Renewable Energies - Laboratory of Applied Physics (LPA-GMTER), Faculty of Sciences, Fanar Campus, Lebanon
2. University Artois, IMT Lille Douai, Junia, University Lille, ULR 4515, Laboratoire de Génie Civil et géo-Environnement (LGCgE), F-62400, Béthune, France

ARTICLE INFO

Article history
Received: 9 March 2022
Revised: 28 March 2022
Accepted: 20 April 2022
Published Online: 10 May 2022

Keywords:
Hollow block
Cavities
Thermophysical properties
Dynamic boundary conditions
3D modelling

ABSTRACT

During both hot and cold seasons, masonry walls play an important role in the thermal performance between the interior and the exterior of occupied spaces. It is thus essential to analyze the thermal behavior at the hollow block's level in order to better understand the temperature and heat flux distribution in its structure and potentially limit as much as possible the heat transfer through the block. In this scope, this paper offers an experimental and numerical in-depth analysis of heat transfer phenomena inside a hollow block using a dedicated experimental setup including a well-insulated reference box and several thermocouples and fluxmeters distributed at the boundaries and inside the hollow block. The block was then numerically 3D modelled and simulated using COMSOL Multiphysics under the same conditions, properties, and dimensions as the experimentally tested block. The comparison between the numerical and experimental results provides very satisfactory results with relative difference of less than 4% for the computed thermal resistance.

1. Introduction

Energy consumption in buildings is strongly increasing lately due to population growth, economic development and improved living standards. These different causes put additional pressure on the energy system. This consumption mainly includes space heating and cooling. For example, the use of heating in Lebanon presents the most interesting share of household energy consumption in Lebanon in 2012, it is approximately almost half of the total energy consumption. And that the equipment rate of air conditioner presents a strong increase from 16% to 55% from 2000 to 2012 [1]. The energy consumption of air conditioning and heating systems depends on several factors,

*Corresponding Author:
Emilio Sassine,
Lebanese University, Habitat and Energy Unit, Group of Mechanical, Thermal and Renewable Energies - Laboratory of Applied Physics (LPA-GMTER), Faculty of Sciences, Fanar Campus, Lebanon;
Email: emilio.sassine@gmail.com

DOI: https://doi.org/10.30564/jbms.v4i1.4500

one of the most important factors is the heat transfer through the building envelope. In this context, the thermal performance in masonry walls is taken into account in this study, especially since the energy efficiency of buildings is an area that has become very important in the context of energy conservation.

Nowadays, hollow blocks are one of the most used materials in building envelopes for what the advantages they offer in terms of cost, ease of implementation, weight, fire resistance, thermal and sound insulation, and acoustic insulation. For example JJ del Coz Díaz et al. [2] presented a comparative nonlinear thermal analysis for a total of eighteen different in situ cast floors by varying both the constituent materials and the shape of the hollow blocks using the finite element method (FEM). They concluded that the overall heat transfer coefficient increases with increasing material conductivity. In addition, there is a growing interest in using materials with good physical properties for energy conservation. Ribeiro et al. [3] analyzed the sound insulation on a masonry wall built with hollow concrete blocks and construction and demolition waste as aggregates using the reverberant chamber method with the aim of providing sound insulation in indoor environments. They concluded that all types of panels increased the weighted sound reduction index. M. Fringuellino et al. [4] described the characteristics of sound transmission through hollow walls, with the aim of analyzing the sound reduction index on several types of walls with different thicknesses and materials, using the equation based on the familiar formula for the normal incidence transmission of a longitudinal wave at the intersection between different materials. They concluded that the material properties of the complex structure of the block can strongly influence the sound reduction index at the low and high frequency. Yang et al. [5] investigated the sound insulation properties of a concrete hollow brick wall through experimental research and theoretical analysis. They concluded that concrete hollow brick not only has excellent mechanical properties but also excellent sound insulation properties due to its rational hole shape design. Fraile-Garcia et al. [6] studied the acoustic behavior of waste-tire rubber concrete bricks, lattice joists and hollow blocks with different proportions of rubber in the mix using the difference between transmitted and emitted levels method. They proved that highly doped elements are an excellent option for isolating low frequency sounds, while intermediate and standard elements are a more attractive option for blocking medium and high frequency sounds.

Numerical heat transfer modeling is necessary to characterize the thermal parameters of the hollow block. Numerical methods allow to apply the heat transfer equation in steady state or dynamic conditions. Díaz et al. [7] used the finite element method (FEM) for the design optimization of lightweight hollow blocks with the aim of saving energy. They concluded that by increasing the number of vertical and horizontal intermediate bulkheads and decreasing the conductivity of the material, they obtained the best thermal efficiency. A. Antar et al. [8] studied numerically the heat transfer through a hollow block. They concluded that with increasing the number of cavities the heat loss decreased, while keeping the block width constant. Urban et al. [9] analyzed the thermal performance of masonry wall systems for six different geometries with different densities by utilizing a finite difference computer modeling. They concluded that the use of lightweight concretes in the production of concrete masonry units is therefore one of the most effective ways to improve their thermal performance. M. Mahmoud et al. [10] developed a computational fluid dynamics (CFD) model, to determine the size and distribution of cavities in building blocks, which can reduce the variation of the heat flux through the walls as much as possible and thus to obtain energy savings in air conditioning. The results showed that the variation of the heat flux depends on the size of the cavities and blocks. Heinrich Manz [11] studied the heat transfer by natural convection of air layers in vertical rectangular cavities using a computational fluid dynamics (CFD) code. This study has provided the starting position for future applications of the code to more complex cases of facade elements. Fogiatto et al. [12] studied the thermal transmittance for different cavity configurations of hollow concrete blocks by performing CFD simulations. The results showed that larger cavities provide the higher transmittance values and that the radiation effect can play an important role in the overall heat transfer through blocks. Zhang et al. [13] analyzed the thermal performance of a hollow concrete wall using MATLAB program. The results showed that by reducing the number of cavities in each row, the thermal performance could be improved. S. Al-Tamimi et al. [14,15] used a finite element analysis using ABAQUS software to determine the optimal hole geometry for concrete bricks that would increase the thermal resistance of the wall and thus reduce electrical energy consumption. They concluded that there is an effect of the hole shape on thermal resistance and then an effect on heat flux reduction. Then, they developed a finite element model (FEM) with the aim of determining the optimal geometry of cavities and their arrangement in concrete masonry blocks to reduce the heat flux. They concluded that the simulation results are promising and indicated that the new optimal cavity geometry design was much better than commercially available cavity blocks. J. Xamán et al. [16]

studied the thermal analysis of a hollow block with/without insulation and reflective roofing materials for 24 h in the hottest and coldest days, considering environmental variables of a Mexican city with warm weather using the finite volume method. The results showed the interest of using the combination of an insulating material and a reflective coating on roofs with hot weather. Chihab et al. [17] numerically investigated the thermal inertia of different roof configurations constructed with traditional concrete blocks used in Morocco with three and six cavities, using the Galerkin finite element method. The results indicated that the combined emissivity and interior heat transfer coefficients have a significant impact on the thermal inertia of the roof. JJ del Coz Díaz et al. [18] described the development of a new type of hollow concrete masonry block unit to minimize its weight based on topological optimization using the finite element method (FEM). The numerical results gave rise to new solutions in masonry construction through proper block pre-design.

In addition to numerical simulations, many experimental methods have been developed by researchers to estimate thermal performance in building envelopes such as thermal conductivity, thermal resistance, under controlled or real conditions. Among these studies, Hu et al. [19] constructed 6 groups of hollow brick model blocks with different filling positions and filling rates using a cold and hot test box, with the aim of improving the insulation performance of hollow brick, in the continuous operation of air conditioning in the cold regions of China in winter. They concluded that with the filling of the hollow block with EPS insulating material is better at improving the insulation performance of the hollow brick block. Wu et al. [20] investigated the mechanical and thermal properties of rectangular hollow blocks using the hot box method. They concluded that the use of this block could not only reduce the energy consumption but also decrease the pressure on the environment.

Finally researchers have studied experimentally and numerically the heat transfer in the building envelope, for example Sassine et al. [22-24] proposed an experimental and numerical analysis of the thermal performance of Lebanese hollow block concrete. Then, they investigated the effect of adding expanded polystyrene (EPS) beads to the solid mixture of hollow block concrete by numerical and experimental approaches. They concluded from the numerical results is that the three-dimensional (3D) model has visualized the heat flux and temperature distribution in the block as well as the air velocity and convective heat exchange inside the cavities of the block. And from the experimental results, they showed that the thermal resistance of the block can almost double by adding 18 g of polystyrene beads to the concrete mix.

This paper focuses particularly on the heat transfer phenomena inside hollow blocks by instrumenting an experimental setup and measuring local temperatures and heat fluxes in a 49 cm × 19 cm × 10 cm hollow block having four rectangular cavities under controlled conditions using the thermostatic baths in an experimental heating box setup. In the first part of the paper, the equivalent thermal properties of the hollow block and the concrete mixture are determined, namely the thermal conductivity, the density, and the specific heat. Then, in the second part, the detailed heat transfer is studied both experimentally and numerically through heat flux sensors and temperature sensors placed across the studied sample.

2. Standard Thermal Characterization Setup

2.1 Description of the Experimental Setup

2.1.1 Experimental Setup

A standard experimental setup is used to determine the thermal properties of building materials in the LGCgE laboratory. The samples are placed horizontally between two aluminum plates and the heat transfer through the hollow block is measured using a fluxmeter method in a well-insulated reference box.

The heat exchange plates are connected by two thermostat baths as shown in Figure 1a. Such that one is connected to the upper plate at a temperature of 25 °C and the other is connected to the lower plate at 15 °C. The flux and temperature measurement are performed by two flux meters of 0.15 × 0.15 m^2 area and two T-type thermocouples, which are placed below and above the sample respectively. The upper plate can be moved vertically with the help of a support that in turn allows keeping this system in place. The thermal properties to be determined are the thermal conductivity (λ) and the specific heat (CP).

The tested samples were wrapped laterally with a recycled wool insulation material as shown in Figure 1b, in order to reduce lateral heat loss and ensure unidirectional heat transfer.

The thermal properties of the hollow block, namely the thermal conductivity (λ) and the specific heat (Cp), were determined using the fluxmetric method (NF EN 12664 [21]), in which the sample is placed between two aluminum plates connected to thermostatic baths allowing to impose controlled boundary conditions on the sample. Two fluxmeters and two thermocouples are placed above

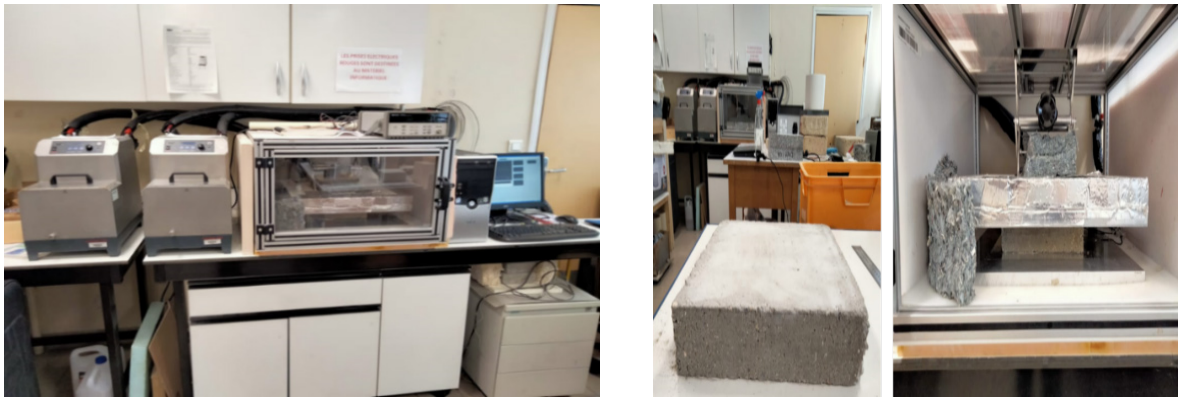

(a) (b)

Figure 1. Experimental setup for thermal characterization

and below the block to measure the heat flux and the temperature respectively. The thermocouples and fluxmeters are connected to a data acquisition center allowing to visualize the evolution of the heat flux and temperature on each face of the block.

2.1.2 Tested Specimens

Two specimens were tested using the standard thermal characterization setup: a concrete mixture sample taken from the hollow block, and the hollow block itself.

To thermally characterize the concrete constituting the hollow block, a sample was prepared by cutting three rectangular pieces from the hollow block and gluing them together using a very thin mortar glue as shown in Figure 2a. The parallelepiped obtained sample is 16.5 cm × 7 cm × 6.5 cm; this provides a sample with sufficient thermal resistance for the measurement method.

(a)

(b)

Figure 2. Tested samples: concrete solid mixture (a) and hollow block (b)

The studied hollow block has a length of 49 cm, a height of 20 cm and a width of 10 cm and contains 4 cavities in series as shown in Figure 2b.

The main ingredients in the production of normal weight hollow block are: natural aggregates, cement and water. The aggregate mixture is made of 25% of fine gravel aggregates (4 mm–8 mm) and 75% of powdered stone dust (0.5 mm–4 mm). The dosage of the mixture is made such as 1 m^3 of aggregates is mixed with 50 kg of Portland cement and 50 L of water to form the solid concrete mixture.

It is a block molded and pressed by a pressing mold in different forms. In our case we considered a block of parallelepiped (24.7 cm × 10 cm × 19cm) and formed by rectangular cavities (Figure 2b).

It is important to highlight that the thermal properties of the hollow block that are determined from experimental measurements are equivalent thermal properties since the

sample is composed of a concrete matrix and air contained in the cavities of the sample.

2.2 Characterization Method

2.2.1 Determination of the Density

The equivalent densities of the samples were determined by dividing weight of the samples (determined using a digital balance) by its volume (length × width × thickness).

2.2.2 Determination of the Thermal Conductivity

The thermal conductivity represents the ability of a material to let heat pass or on the contrary to oppose to it. Because of the difference in temperature on each side of the sample under test, a heat transfer exchange exists. Once the steady state is reached, one can calculate the thermal conductivity (λ) such as $\lambda = \frac{e}{R}$ with e is the thickness of the sample studied in m, R is the thermal resistance in $m^2.K/W$, and λ is the thermal conductivity in $W/m.K$. Then the higher the thermal conductivity, the more heat the material allows to pass and therefore it is less insulating.

The flux and temperature were measured simultaneously on each block face and then the resistance R was calculated using Fourier's law in a unidirectional steady state system, such as;

$$\varphi_1 = \frac{\Delta\theta}{R} \tag{1}$$

$$\varphi_2 = \frac{\Delta\theta}{R} \tag{2}$$

$\Delta\theta$ is the temperature difference.

Once we determine the flux variation, we can calculate its sum $\Sigma\varphi$, and then the thermal resistance R, such that;

$$\Sigma\varphi = \frac{2}{R}\Delta\theta \tag{3}$$

$$\Longrightarrow R = \frac{2\,\Delta\theta}{\Sigma\varphi} \tag{4}$$

Finally, we can calculate the thermal conductivity, using the following formula;

$$\lambda = \frac{e}{R} \tag{5}$$

The thermal conductivity is determined when the sum of the fluxes stabilizes.

2.2.3 Determination of the Specific Heat

The specific heat C_P is designated by the amount of heat stored in a material, i.e. it is expressed by the heat capacity C. This means that when the heat capacity increases, a large amount of energy can be stored but the temperature becomes less important. Note that for the same sample the value of the specific heat varies with the temperature.

This amount of energy Q can be calculated from an initial state $t_{initial}$ steady state and then changing the temperature set point on one or both sides, so that our system reaches the steady state again, in which the material has returned to its stable state at a final state t_{final}, we can calculate Q;

$$Q = \int_{t_{initial}}^{t_{final}} \Delta\varphi \, dt \tag{6}$$

$\Delta\varphi$ expresses the difference in fluxes. dt denotes the time step, in our case we considered $dt = 10\ sec$. Q is the energy stored in the sample during the transient phase, it is expressed in J.

As well as, the heat capacity (C) is obtained by dividing the amount of energy supplied (Q) by the temperature difference ($\Delta\theta$), such that;

$$C = \frac{Q}{\Delta\theta} \tag{7}$$

C is expressed in (J/K), $\Delta\theta$ presents the difference between the average temperature in the final state and the average temperature in the initial state, i.e. that;

$$\Delta\theta = \overline{\theta_{final}} - \overline{\theta_{initial}} \tag{8}$$

If the heat capacity increases, this means that a large amount of energy can be stored, relatively low temperature.

Finally, knowing the heat capacity C, the density of the sample ρ and its thickness e, then;

$$C_P = \frac{C}{\rho.S.e} \tag{9}$$

ρ is expressed in $kg/m3$, S is the surface area of the sample in m^2, e is the thickness of the tested sample in m, C_P is the specific heat capacity expressed in $J/Kg.K$.

Note that the specific heat C_P is different for each material and according to the physical state (solid, liquid and gas).

The specific heat is determined when the difference of the flux is stable.

2.3 Experimental Results

2.3.1 Thermal Properties of the Concrete Mixture

The concrete solid mixture of the block sample has a density of ρ = 2150 Kg/m^3.

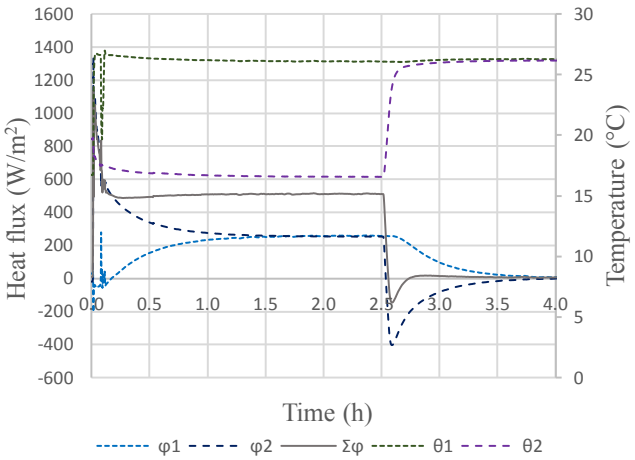

(a)

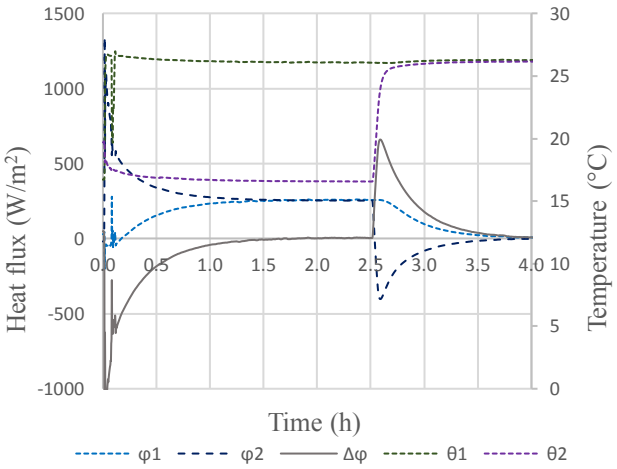

(b)

Figure 3. Determination of thermal conductivity (a) and the specific heat (b) of the concrete mixture

At first, a different temperature difference was imposed such that θ_1=25 °C and θ_2= 15 °C, in order to determine the thermal conductivity of the sample. After 1h30, the steady state is reached and the heat fluxes at the boundaries of the sample φ_1 and φ_2 are approximately equal to 254 W/m^2 (Figure 3a). After reaching the steady state conditions, the temperature condition θ_2 is increased to 25 °C, in order to determine the specific heat of the sample. The heat fluxes φ_1 and φ_2 decrease and converge to an approximately zero value (Figure 3b).

By using Equations (4), (5) and (9) the thermal conductivity and the specific heat can be computed: λ = *1.6 W/m.K* and C_P = *1392.82 J/m.K*.

2.3.2 Equivalent Thermal Properties of the Hollow Block

The density equivalent density of the hollow block is

$$\rho = \frac{m}{V} = \frac{11.3}{0.49x0.19x0.1} = 1213.75\ Kg/m^3.$$

Two tests were performed for the determination of the thermal properties of the hollow block. In the first one (1), the two fluxmeters were placed in the middle of the block on both sides of the block. In the second (2), the fluxmeters are placed on both sides of the cavity as shown in Figure 4.

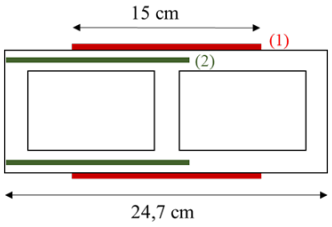

Figure 4. Fluxmeters locations in the two tests

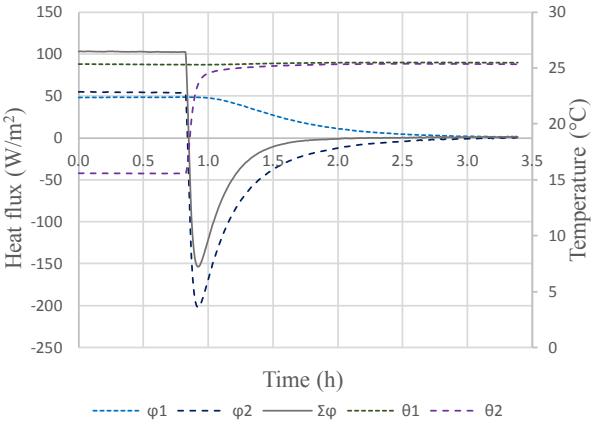

(a)

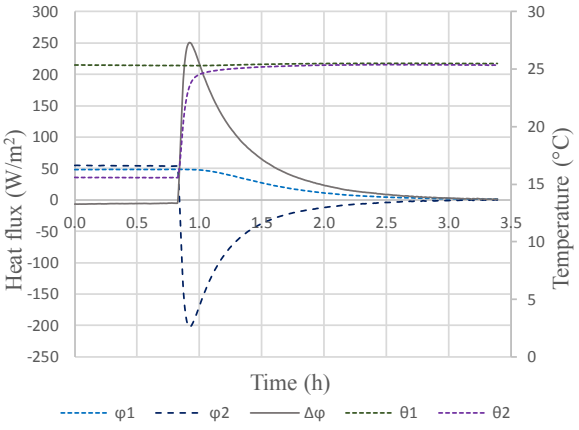

(b)

Figure 5. Determination of thermal conductivity (a) and the specific heat (b) of the hollow block in the 1st test

According to Equations (4) and (5) and Figure 6a;

$R = \frac{2\Delta\theta}{\Sigma\varphi} = \frac{2x9.77}{104} = 0.188\ m^2.K/W$

$\Rightarrow \lambda = \frac{e}{R} = \frac{0.1}{0.188} = 0.53\ W/m.K$.

From Equation (9) and Figure 6b, $C_P = \frac{C}{\rho.S.e} = \frac{92107.57}{1213.96x1x0.1} = 758.73\ J/Kg.K$.

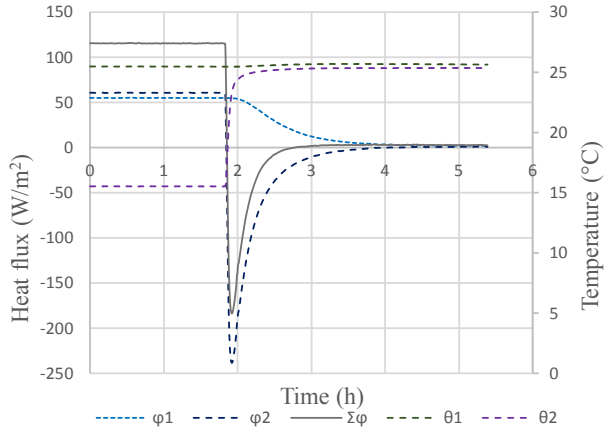

(a)

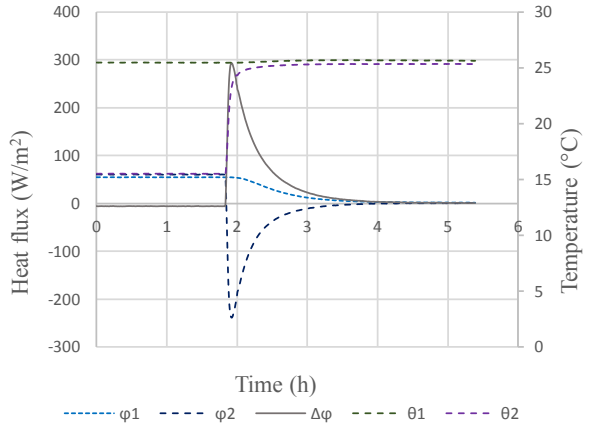

(b)

Figure 6. Determination of thermal conductivity (a) and the specific heat (b) of the hollow block in the 2nd test

According to Equations (4) and (5) and Figure 6a, $R = \frac{2\Delta\theta}{\Sigma\varphi} = \frac{2x9.9}{115} = 0.172\ m^2.K/W \Rightarrow \lambda = \frac{e}{R} = \frac{0.1}{0.172} = 0.58\ W/m.K$.

According to Equation (9) and Figure 6b $C_P = \frac{C}{\rho.S.e} = \frac{99971.01}{1213.96x1x0.1} = 823.51\ J/Kg.K$

So far, as a first conclusion, the thermal conductivity obtained in test 2 is approximately greater than that in the first one. This can be justified by the fact that in the second test, the fluxmeters were placed on two sides where there are more materials.

Table 1 summarizes all the thermal properties of the tested samples. The results show that the location of the sensors between tests 1 and 2 has a slight impact on the thermal conductivity (8%) and the specific heat (8%).

Table 1. Thermal properties of the tested materials

Material	ρ (Kg/m^3)	λ (W/m.K)	C_p (J/Kg.K)
Hollow block (configuration 1)	1214	0.53	758.73
Hollow block (configuration 2)	1214	0.58	823.51
Concrete mixture	2150	1.6	1393

3. Detailed Heat Transfer Phenomena in the Hollow Block

3.1 Description of the Experimental Setup

After the determination of the equivalent thermal properties of the block and the solid part of the hollow block, a particular attention was given to the analysis of the heat transfer inside the hollow block. A particular experimental setup was built for this purpose where the block was placed between two flat plates and the assembly was well insulated using polyurethane and wood to ensure a unidirectional transfer in the system (Figure 7).

The temperature in the box varies in a step shape between 10 °C and 50 °C. It is covered by 16 cm of polyurethane insulation and 1.5 cm of wood on the borders of the box.

The block is well insulated to ensure a unidirectional heat transfer created by the difference in temperature between the two edges of the block from the hotter side to the colder side.

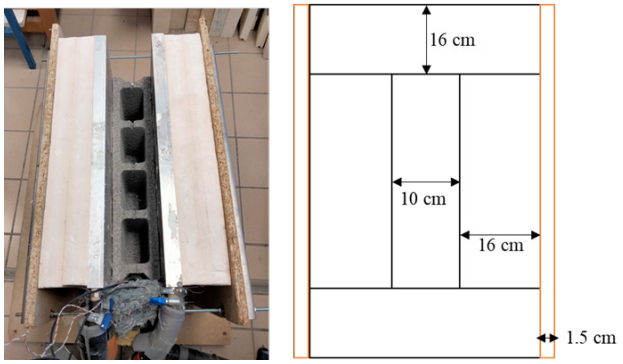

(a) (b)

Figure 7. Photography (a) and schematic cross section (b) of the experimental setup

3.1.1 Measuring Devices

A thermocouple is a sensor that consists of measuring the temperature at a particular point, i.e. it is used to measure the temperature in the form of an electric current or an electromotive force. This measurement is based on

the Seebeck effect.

Indeed, a thermocouple is composed by two wires of different metals which are joined at the ends. Then, the latter creates a junction so that the temperature is measured. There are different types of thermocouples, each corresponding to a different temperature range and a different accuracy.

In our experiment we used T-type thermocouples (Copper-Constantan), in order to measure the temperature in the cavities and on both sides of the block. This thermocouple is suitable for a temperature range between –250 °C and 400 °C. It can be used at a low temperature, such as in cryogenic applications.

The block is placed vertically between two aluminum plates, such that each plate is connected to a thermostat bath. Each bath is set at a different temperature; the first is at 10 °C and the other one varies between 10 °C and 50 °C. Then, 16 T-type thermocouples were placed in the cavities of the block using small wooden rods and on the faces of the cavities. Finally, these thermocouples are connected to an acquisition center to determine the temperature variation inside the cavities.

3.1.2 Distribution of the Sensors

16 T-type thermocouples were placed; 5 thermocouples (12, 13, 14, 15 and 16) are placed at 9 cm at the end of the block such that 3 of them are placed in the cavities (13, 14 and 15). In addition, 6 thermocouples are placed at 19 cm and 28 cm respectively from the extremity of the block (1, 2, 3, 4, 5 and 6). Finally, 5 sensors are placed at 38 cm from the extremity of the block; such that 7 and 11 are placed on the faces of the block respectively and 8 9 and 10 are placed in the cavities. All sensors are placed at a height of 9 cm from the vertical section of the block, as in (Figure 8).

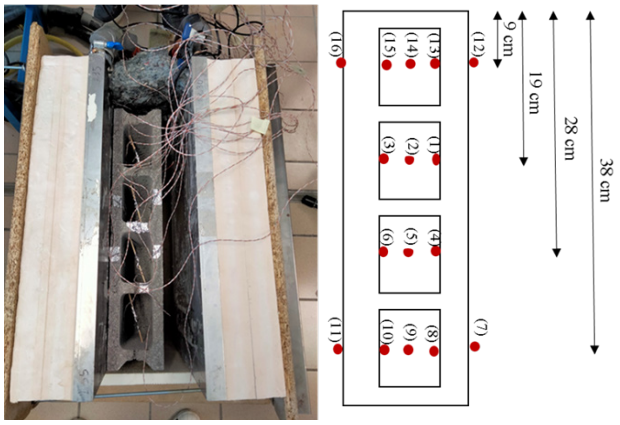

Figure 8. Distribution of thermocouples across the hollow block

3.2 Imposed Boundary Conditions

Temperature boundary conditions (Dirichlet conditions θ_1 and θ_2) were applied on the two faces of the block through heat exchange plates connected to thermostatic baths. While θ_1 remains constant approximately at 20 °C, θ_2 varies in a steep temperature profile between 20 °C and 50 °C over a period of 5 days. Moreover, the comparison between the experimental and numerical results was given a particular attention.

3.3 Numerical Model

Numerical simulations were carried out using COMSOL® version 5.6 software. In this 3D study, a structured mesh was considered using transient heat transfer.

Other the understand of the heat transfers by convection and thermal radiation that are taken into account in our numerical model on this type of concrete block that contains four rectangular cavities, the difficulty and interest of our study is the air flow inside the cavities, considering the natural convection as a laminar flow. Therefore, two physical parameters have been considered in our model; "Laminar Flow" and "Heat Transfer in Fluids". The continuity, Navier-Stokes and energy equations have been used in our model.

The 3D block model is the same as the experimentally tested block; it is composed of a row of four rectangular cavities of 9.5 × 19 × 6 cm^3. The external dimensions of the block are 49 × 19 × 10 cm^3 (Figure 9).

The size, dimensions and boundary conditions of the block in the numerical analysis are identical to the experimental in transient regime. An initial condition of $\theta 0 = 20\ °C$ and a time step of 1 min were considered. The sensors are placed in the numerical model are the same as the ones placed in the experimental analysis with the aim of comparing the results of these two analyses.

The heat transfer simulation in hollow blocks is based on the thermal properties of the concrete mixture presented in Table 1. A coupled CFD-thermal analysis was adopted in order to account the three key heat transfer mechanisms of the (i.e., conduction, convection, and radiation).

The conduction occurs in the solid concrete mixture of the hollow block, while convection and radiation occur inside the block cavities. The air circulation inside the cavity (Figure 9a), promoting the natural convection, was considered as a laminar flow. It is coupled with the radiation model using the discrete ordinates method (DO) and the simulation was performed using the implicit solver of COMSOL Multiphysics®. The air density was assumed to be dependent on pressure and temperature varying according to the ideal gas relation [22-24].

The equivalent thermal properties of the solid part of the block; λ=1.6*W/m.K* and C_P=1392.82 *J/Kg.K* have been taken into account in our numerical models (Figure 9b).

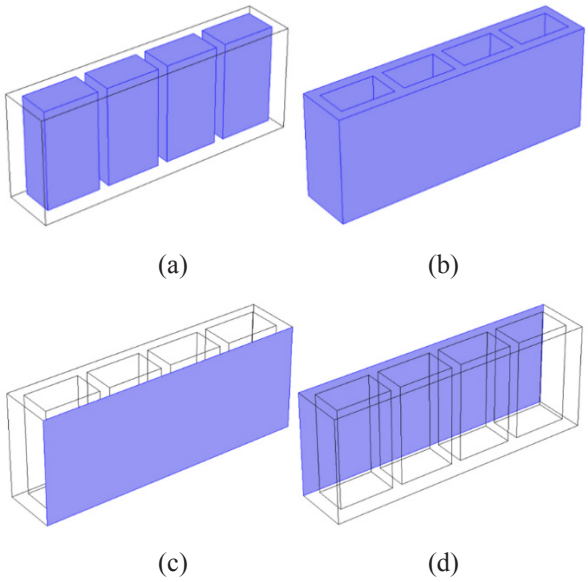

(a) (b)

(c) (d)

Figure 9. Materials constituting the block air (a) concrete (b) and boundary conditions θ_1 (c) et θ_2 (d)

The boundary conditions that we have considered are the boundary conditions of those of the experimental part; θ_1 and θ_2 (Figure 9c and Figure 9d).

In order to compare the experimental measurements of temperature and heat flux in the hollow block with the numerical 3D simulations, the numerical model sensors were placed at the same coordinates as those of the experimental setup. Figure 10 shows the location of sensors S2, S4, and S11 as example.

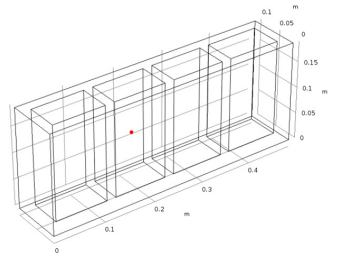

(a)

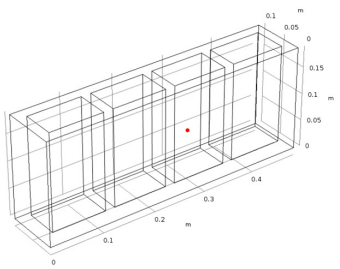

(b)

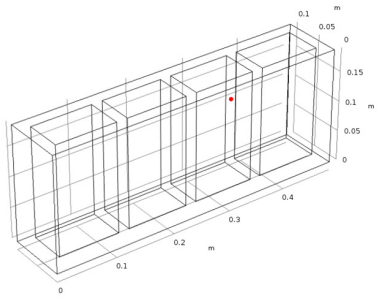

(c)

Figure 10. Sensor coordinates S2 (a) S4 (b) S11 (c)

3.4 Comparison between the Numerical and Experimental Results

The main objective of comparing numerical and experimental results is providing a solid understanding of the heat flux in hollow blocks in dynamic conditions at the boundaries of the hollow block as well as at its mesostructured (inside the cavities).

Figure 11 and Figure 12 show the evolution of temperature at the left and right boundaries of the block. The numerical results and the experimental measurements present a very good agreement. The results also show that the temperature is relatively uniform at the block edges since the difference between θ_2, S11, and S16 does not exceed 2 degrees. This slight difference is due to the edge effects; indeed, the small size of the studied sample prevents the variation of the heat flux to be perfectly unidirectional. The same differences are observed between sensors θ_1, S7, and S12.

The temperature on the left side increases and presents a step form due to the increase in the heat exchanging plates reference temperature (step profile 20 °C-30 °C-40 °C-50 °C); the temperature on the right side is slightly affected since it shows a little increase while the heat exchanging plate at that side is maintained at 20 °C.

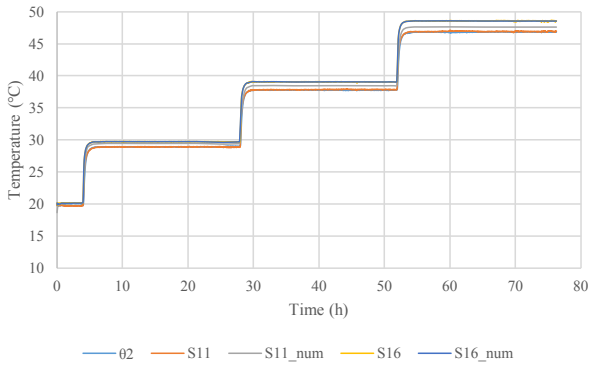

Figure 11. Comparison between numerical and experimental temperatures of sensors 11 and 16 at the left boundary of the block

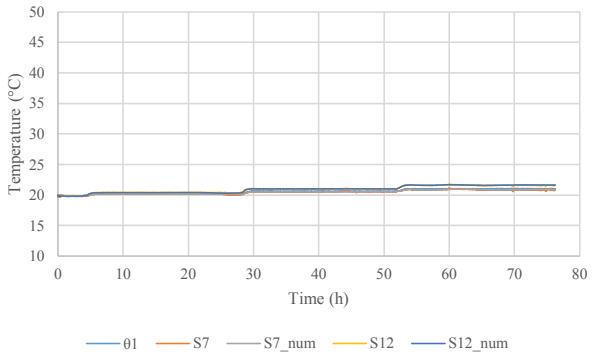

Figure 12. Comparison between numerical and experimental temperatures of sensors 7 and 12 at the right boundary of the block

The temperature measurements inside the cavities are shown in Figure 13, Figure 14, and Figure 15. The edge effects are more pronounced at the internal edges of the cavities (left and right side) and almost absent in the middle of the cavities.

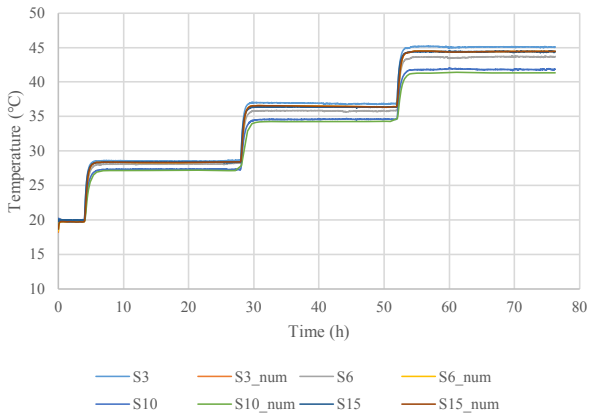

Figure 13. Comparison between numerical and experimental temperatures of sensors 3, 6, 10 and 15 at the left internal edge of the cavities

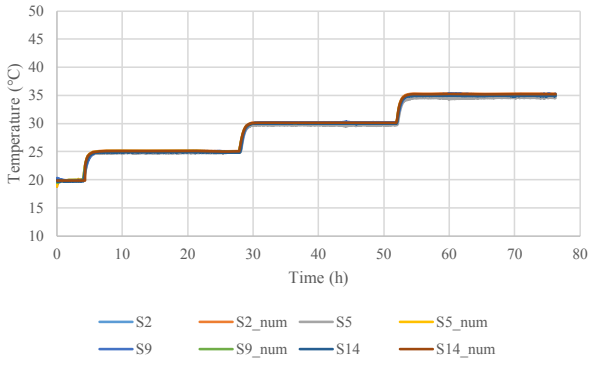

Figure 14. Comparison between numerical and experimental temperatures of sensors 2, 5, 9 and 14 at the middle of the block cavities

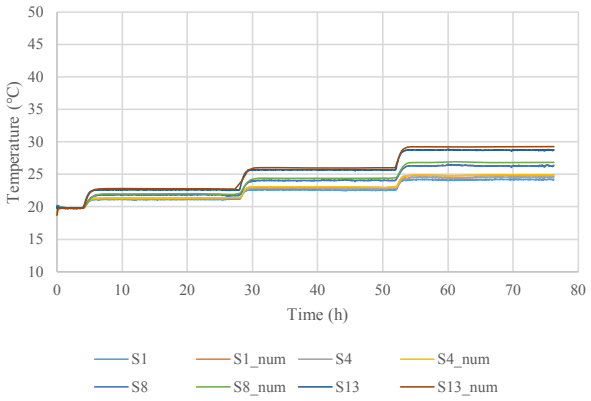

Figure 15. Comparison between numerical and experimental temperatures of sensors 1, 4, 8 and 13 at the right internal edge of the cavities

The heat flux measurements on the two interfaces of the block/heat exchanging plates were compared to numerical simulations (Figure 15). The results of the heat flux evolution are very comparable for the two sides of the hollow block. While the heat flux from the hot side peaks for each change in the temperature range and then decreases until reaching a new constant range, the heat flux from the cold side (20 °C) increases in a smoother way until reaching the new steady state value for each increase of the temperature range from the hot side. Furthermore, the computation of the numerical and experimental thermal resistances obtained from the numerical and experimental results respectively and reported in Table 2 show a great adequacy with a relative difference less than 4% for the three measurement ranges. The thermal resistance decreases with the increase of the temperature difference between the two boundaries of the hollow block from 0.148 m^2.K/W to 0.135 m^2.K/W in the numerically simulated block and from 0.142 m^2.K/W to 0.131 m^2.K/W for the experimental measurements. These results are also in compliance with the previous similar studies performed on similar hollow block with two rows of elliptical cavities [22] where the thermal resistance of a 10 cm × 20 cm × 40 cm hollow block was found equal to 0.151 m^2.K/W and in compliance with French thermal regulations RT 2012 [25] stating that the thermal resistance of a 10 cm × 20 cm × 50 cm hollow block with one row of squared hollows shall be taken equal to 0.12 m^2.K/W.

The conclusions drawn from the experimental and numerical comparisons are as follows:

A good match between numerical and experimental results can be confirmed which consolidates the numerical model allowing further investigations of heat transfer in hollow blocks having different shapes and different concrete mixtures.

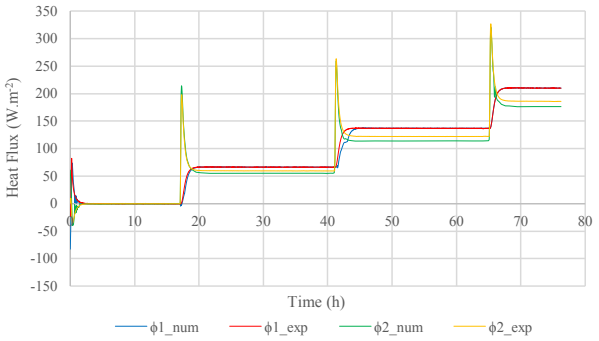

Figure 15. Comparison between numerical and experimental heat fluxes at 13 at the external faces of the hollow block

Table 2. Thermal properties of the tested materials

Temperature (°C)	20-30 °C	20-40 °C	20-50 °C
$R_{experimental}$ (m^2.K/W)	0.142	0.135	0.131
$R_{numerical}$ (m^2.K/W)	0.148	0.140	0.135
Relative deviation	4%	4%	2%

The temperature gradient inside the block decreases progressively from the side where the step temperature θ_2 is applied to the side where a constant temperature θ_1 is imposed.

The heat flux on the two boundaries of the tested hollow block was also measured and simulated showing comparable results.

Edge effects are observed at the boundaries of the block and at the internal edges of the cavities and are almost absent in the middle of the cavities. These effects can be reduced by working on a wall scale (masonry walls).

The thermal resistance of the block was always investigated for different temperature ranges and using both experimental measurements and numerical simulations showing a very high adequacy between the numerical and experimental values.

4. Conclusions

This work provides an in-depth understanding of heat transfer in hollow concrete blocks by investigating the local temperature distribution and heat flux through an experimented hollow block with rectangular cavities using the fluxmetric method under controlled conditions in a well-insulated experimental box.

The thermal properties of the hollow block and the solid matrix were first determined using a standard thermal characterization setup. Two tests were made; in the 1st test the two fluxmeters were placed in the middle of the tested block facing the bulkheads on both sides, whereas in the 2nd test, the two flux meters were placed facing the centers of the cavities on both sides.

In the second section of the paper, a detailed thermal analysis of the hollow block was performed by imposing a constant temperature condition on one side of the block, the other side being imposed to a step temperature profile which varying between 20 °C and 50 °C. The hollow block that was placed vertically between the heat exchanging plates and sixteen thermocouples and two fluxmeters were distributed inside and at the boundaries of the block to record the temperature and heat flux evolution.

A numerical study was also performed to support and validate the measurements; a 3D model of the block was produced and numerical sensors were placed in the same locations as the experimental configuration.

After validating the heat transfer experimental and numerical models, the scope of the upcoming work will be to improve the thermal performance of the block by modifying the concrete mixture composition, or by modifying the block internal geometry, or by filling the block cavities by insulation materials.

Conflict of Interest

There is no conflict of interest.

References

[1] Energie, changement climatique et bâtiment en Méditerranée : étude nationale Liban - Plan-bleu : Environnement et développement en Méditerranée. https://planbleu.org/publications/energie-changement-climatique-et-batiment-en-mediterranee-etude-nationale-liban/

[2] del Coz Díaz, J.J., García Nieto, P.J., Domínguez Hernández, J., et al., 2010. A FEM comparative analysis of the thermal efficiency among floors made up of clay, concrete and lightweight concrete hollow blocks. Applied Thermal Engineering. 30(17), 2822-2826.
DOI: https://doi.org/10.1016/j.applthermaleng.2010.07.024

[3] Ribeiro, R.S., Sousa, R.P.D., Amarilla, R.S.D., et al., 2021. Sound insulation of a hollow concrete blocks wall made with construction and demolition waste and wood-based panels as linings. Building Acoustics. 28(4), 423-442.
DOI: https://doi.org/10.1177/1351010X21993640

[4] Fringuellino, M., Smith, R.S., 1999. Sound Transmission through Hollow Brick Walls. Building Acoustics. 6(3), 211-224.
DOI: https://doi.org/10.1260/1351010991501419

[5] Yang, W., Mai, G., Yang, R., 2004. Study of sound

insulation properties of concrete hollow brick wall. https://www.semanticscholar.org/paper/STUDY-OF-SOUND-INSULATION-PROPERTIES-OF-CONCRETE-Yang-Mai/a428e48490ca7694b5b-31c75058fd50bcea6a5aa.

[6] Fraile-Garcia, E., Ferreiro-Cabello, J., Defez, B., et al., 2016. Acoustic Behavior of Hollow Blocks and Bricks Made of Concrete Doped with Waste-Tire Rubber. Materials (Basel). 9(12), 962. DOI: https://doi.org/10.3390/ma9120962

[7] del Coz Díaz, J.J., García Nieto, P.J., Domínguez Hernández, J., et al., 2009. Thermal design optimization of lightweight concrete blocks for internal one-way spanning slabs floors by FEM. Energy and Buildings. 41(12), 1276-1287. DOI: https://doi.org/10.1016/j.enbuild.2009.08.005

[8] Antar, M.A., Baig, H., 2009. Conjugate conduction-natural convection heat transfer in a hollow building block. Applied Thermal Engineering. 29(17), 3716-3720. DOI: https://doi.org/10.1016/j.applthermaleng.2009.04.033

[9] Urban, B., Engelmann, P., Kossecka, E., et al., 2011. Arranging Insulation for Better Thermal Resistance in Concrete and Masonry Wall Systems. 3, 8.

[10] Mahmoud, M., Ben-Nakhi, A., Ben-Nakhi, A., et al., 2012. Conjugate conduction convection and radiation heat transfer through hollow autoclaved aerated concrete blocks. Journal of Building Performance Simulation. 5(4), 248-262. DOI: https://doi.org/10.1080/19401493.2011.565886

[11] Manz, H., 2003. Numerical simulation of heat transfer by natural convection in cavities of facade elements. Energy and Buildings. 35(3), 305-311. DOI: https://doi.org/10.1016/S0378-7788(02)00088-9

[12] Fogiatto, M.A., Santos, G.H., Mendes, N., 2016. Thermal transmittance evaluation of concrete hollow blocks. Undefined. [online]. Available on: https://www.semanticscholar.org/paper/Thermal-transmittance-evaluation-of-concrete-hollow-Fogiatto-Santos/f59a619a72d9a1b0640e6e75189c434fd33be95d

[13] Zhang, Y., Wang, Q., 2017. Influence of Hollow Block's Structural Configuration on the Thermal Characteristics of Hollow Block Wall. Procedia Engineering. 205, 2341-2348. DOI: https://doi.org/10.1016/j.proeng.2017.10.306

[14] Al-Tamimi, A.S., Baghabra Al-Amoudi, O.S., Al-Osta, M.A., et al., 2020. Effect of insulation materials and cavity layout on heat transfer of concrete masonry hollow blocks. Construction and Building Materials. 254, 119300. DOI: https://doi.org/10.1016/j.conbuildmat.2020.119300

[15] Al-Tamimi, M., Al-Osta, O., Al-Amoudi, R., et al., 2017. Effect of Geometry of Holes on Heat Transfer of Concrete Masonry Bricks Using Numerical Analysis. Arabian Journal for Science & Engineering. 42. DOI: https://doi.org/10.1007/s13369-017-2482-6

[16] Xamán, J., Cisneros-Carreño, J., Hernández-Pérez, I., et al., 2017. Thermal performance of a hollow block with/without insulating and reflective materials for roofing in Mexico. Applied Thermal Engineering. 123, 243-255. DOI: https://doi.org/10.1016/j.applthermaleng.2017.04.163

[17] Chihab, Y., Essaleh, L., Bouferra, R., et al., 2021. Numerical study for energy performance optimization of hollow concrete blocks for roofing in a hot climate of Morocco. Energy Conversion and Management. 12, 100113. DOI: https://doi.org/10.1016/j.ecmx.2021.100113

[18] del Coz Díaz, J.J., García Nieto, P.J., Álvarez Rabanal, F.P., et al., 2011. Design and shape optimization of a new type of hollow concrete masonry block using the finite element method. Engineering Structures. 33(1), 1-9. DOI: https://doi.org/10.1016/j.engstruct.2010.09.012

[19] Hu, W., Xia, Y., Li, F., et al., 2021. Effect of the filling position and filling rate of the insulation material on the insulation performance of the hollow block. Case Studies in Thermal Engineering. 26, 101023. DOI: https://doi.org/10.1016/j.csite.2021.101023

[20] Wu, J., Bai, G., Zhao, H., et al., September 2015. Mechanical and thermal tests of an innovative environment-friendly hollow block as self-insulation wall materials. Construction and Building Materials. 93, 342-349. DOI: https://doi.org/10.1016/j.conbuildmat.2015.06.003

[21] National standards and national normative documents, July 2001. Thermal performance of building materials and products - Determination of thermal resistance by means of guarded hot plate and heat flow meter methods - Dry and moist products of medium and low thermal resistance.

[22] Sassine, E., Cherif, Y., Dgheim, J., et al., 2020. Experimental and Numerical Thermal Assessment of Lebanese Traditional Hollow Blocks. International Journal of Thermophysics. 41(4), 47. DOI: https://doi.org/10.1007/s10765-020-02626-7

[23] Sassine, E., Cherif, Y., Dgheim, J., et al., 2020. Experimental and Numerical Thermal Assessment of

EPS Concrete Hollow Blocks in Lebanon. Journal of Materials in Civil Engineering. 32(8), 05020007. DOI: https://doi.org/10.1061/(ASCE)MT.1943-5533.0003335

[24] Sassine, E., Cherif, Y., Dgheim, J., et al., 2020. Investigation of the mechanical and thermal performances of concrete hollow blocks. SN Applied Sciences. 2(12), 2006. DOI: https://doi.org/10.1007/s42452-020-03881-x

[25] RÉGLEMENTATION THERMIQUE, 2012. RÈGLES Th-U, FASCICULE 4: PAROIS OPAQUES, CSTB.

BILINGUAL PUBLISHING CO.
Pioneer of Global Academics Since 1984

Journal of Building Material Science
https://ojs.bilpublishing.com/index.php/jbms

ARTICLE

Influence of Pre-saturation of Gravel on the Mechanical Properties of Concrete

Habeeb Solihu Abdulwasiu Abdulkadir*

Institute of Technology, Kwara State Polytechnic, Ilorin, Kwara State, Nigeria

ARTICLE INFO

Article history
Received: 10 June 2022
Revised: 30 June 2022
Accepted: 11 July 2022
Published Online: 20 July 2022

Keywords:
Natural aggregate
Pre-saturated aggregate
Compressive strength
Mechanical properties

ABSTRACT

In this study, the laboratory tests on the influence of pre-saturation of gravel on the mechanical properties of concrete were carried out. The study accessed the specific gravity, water absorption capacity, the impact and the crushing values of the coarse aggregates. Also, this study determined and compared the compressive strengths of concrete produced with the pre-saturated gravel and the dry natural gravel. The results of the compressive strength comparisons have revealed that about 10.8%, 5.6%, 9.4%, and 28.4% reductions in compressive strengths when the samples prepared with pre-saturated and natural aggregates were crushed at 7 days, 14 days, 21 days, and 28 days curing periods respectively. Thus, pre-saturation of aggregate has a negative impact on the strength of the concrete. This study recommends that the pre-saturated aggregate be avoided/treated as much as possible in concrete production because it has a negative impact on the compressive strength of the concrete. That is, it reduces the compressive strength at different curing periods.

1. Background of the Study

Concrete is a commonly used important materials in modern civil engineering structures [1]. It is a world's most frequently utilized building materials, significantly more than any other material in the construction industry. Concrete when compared to other forms of materials used in construction, it is a commonly and predominantly used constructional materials [2]. Besides meeting the requirement of high compression and tension-resistances, concrete is easy to construct, and its high strength, toughness and impermeability can be maintained for a long time [1].

Pre-saturation methods of coarse aggregate intend to minimize as much as possible the exchange of water between the cement paste and the aggregate. Authors such as Hansen [3] observed that aggregate should be saturated completely to stop any water transfer into the aggregates. However, Barra et al. [4] suggest that saturation point should not reached because of the risk of bleeding

*Corresponding Author:
Abdulwasiu Abdulkadir,
Institute of Technology, Kwara State Polytechnic, Ilorin, Kwara State, Nigeria;
Email: abdulkadir.a@kwarastatepolytechnic.edu.ng

DOI: https://doi.org/10.30564/jbms.v4i1.4780

i.e. the transfer of water from within the aggregates to the cement paste, which could impact the water/cement ratio in the interfacial transition zone (ITZ) between the coarse aggregate and the cement paste, affecting the bond strength. The influence of the microstructure of ITZ in concrete mechanical behavior, depending on surface properties and pore structure of coarse aggregate has been pointed out [5].

Concrete is a brittle material with low tensile and high compressive strengths. Thus, to handle the tensile stresses, reinforcement in forms of steel bars is imperative in concrete. Steel is one of the most vital and indispensable material in construction activity [2]. Over 3 million scientific papers are written every year and more than 5 thousand are involved with concrete [6]. Concrete is the most widely used construction material due to its high stability, availability and low cost. Structural properties of concrete such as strength, ductility, elasticity, creep resistance, and durability, have been intensively-studied [7].

Traditionally, other materials are also being used as major building materials in construction sector [8]. However, in recent years, alternative and sustainable cement based materials have attracted serious attention both in the industry and the academic rim [9,10]. The effect of the pre-saturation of the recycled coarse concrete aggregate (RCCA) on concrete's fresh and hardened properties produced using the mixing water compensation method was investigated and compared with a conventional concrete. Both methods can be easily adopted at concrete plants or construction sites [11].

According to Pierre-Claude [12], concrete, the most widely used construction material, is evolving. Modern concrete is more than just a mixture of cement, fine, and coarse aggregates; modern concrete contains more of superplasticizers (SP), chemical admixtures, fibers, and etc. The development of these smart concretes results from the use of sophisticated scientific apparatus and the emergence of a new science of concrete to observe concrete microstructure and even nanostructure.

Also, Cartuxo et al. [13], investigated the influence of two SPs on the rheological behaviour of concrete made with fine recycled concrete aggregates (FRCA). Three families of concrete were tested. Five replacement ratios (0%, 10%, 30%, 50% and 100%) of natural sand by FRCA were tested. The results show that the incorporation of FRCA significantly increased the shrinkage and creep deformation.

According to a study [10], with the demand for environmental sustainability, and for producing more durable and sustainable concrete, attention is paid to the production of concrete with Portland cement substituted by alternative binder materials. Recently, the continuously depletion of the ozone layer and global warming issue have increased the awareness of the construction industries in using more eco-friendly construction materials. Geo-polymer concrete has started to gain significant attention in research community, due to its benefits in using by-product waste to replace cement and reducing greenhouse gas emission during its production. It also possesses better mechanical properties and durability compared to conventional concrete [14].

Barra et al. [4] tested several concrete with different incorporation ratio of gravel at an oven dried (OD), air dried (AD) (approximately 90% of water content) and saturated surface dried (SSD) moisture state to compressive strength, flexural strength and freeze-thaw resistance and using super plasticizes to maintain workability, verified that concrete with air dried gravel presented the best results. These authors obtained the air after saturation. Later, Poon et al. [5] also, tested several concrete with aggregate at oven dried (OD), air dried (AD), and saturate surface dried (SSD) states but without the use of plasticizers and maintain the effective water cement ratio in mixes by adding extra water in order to reach aggregate saturation. Test performed on slump and compressive strength and concrete with air dried aggregates had no preparation and were used as received in laboratory (at about 50% of potential water content).

Again, Rodrı´guez-Robles [15] opined that, the use of construction and demolition waste in concrete manufacture allows the concept of sustainability to be included in the construction industry and helps to alleviate both the large consumption of natural resources and the high generation of waste. The secondary material characterization shows that, despite presenting promising properties in terms of granulometry, particle size, density and shape, the recycled aggregates (RA) should be pretreated to comply with the quality of fineness and water absorption, and their resistance to fragmentation limits their application in concrete mixes with a strength grade below 30 MPa. The results on the hardened concrete revealed that the use of mixed RA is feasible, but at the expense of minor losses of the mechanical characteristics.

Also, [16] by experimenting a two stage mixing against traditional mixing induced a pre-saturation to the coarse aggregate which result in higher compressive strength concretes. The results were explained by the authors as the consequence of a better interfacial transition zone caused by the filling of coarse aggregate surface pores with a denser cement paste.

Etxeberria et al. [17], therefore, recommend an 80% pre-saturation of the potential water content in coarse

aggregate. Coarse aggregate can be pre-saturated by immersion in the water for a determined period of time. The aggregate surface should however, be dry because any surface water could increase the water cement ratio. The challenges with guaranteeing this condition on a large scale suggested the use of sprinklers in aggregate piles in the plant. Meanwhile Lima [18] opined that there would be issues of homogeneity and the possibility of smaller particles being washed away.

Therefore, investigating the laboratory influence of pre-saturation of gravel on the mechanical properties of concrete is the rationale for this study. The study determined the specific gravity, water absorption capacity, the impact value and the crushing value of the gravel. The properties of fresh concrete such as the workability of concrete is an important factor contributing to the strength of concrete. This workability can be altered by the amount of water absorbed by the gravel during pre-saturation. This study determined and compared the compressive strengths of concrete produced with pre-saturated gravel and dry natural gravel. Thus, in order not to negatively affect the characteristics of both fresh and hardened concrete when pre-saturated aggregate is being used, carrying out this project is justified.

2. Materials and Methods

2.1 Materials Used

Natural gravel was used as the coarse aggregate. Sharp sand was used as the fine aggregate while Dangote Ordinary Portland cement was used as the concrete binder. Potable water was used for concrete mixing during production and for concrete curing.

Material Quantification

Bill of quantity is defined as the means of estimating the quantities of the individual components of concrete such as the cement, water, fine, coarse aggregates in accordance with the chosen design mix ration. This study estimated the quantities of the materials needed before batching. Batching by weight is a method of batching where the individual concrete components were measured relative to their weights for a chosen mix ratio. So, for this study, batching by weight was used because it is believed to be more accurate relative to the other method of batching (batching by volume).

2.2 Sieve Analysis

Sieve analysis is a laboratory test commonly used to determine the particle size distributions for the fine and the coarse aggregates components of concrete. The apparatus and the procedures followed are described as follows.

Apparatus:

- Fine aggregate
- Coarse aggregate
- Set of sieves of different sizes as shown in Plate 1.

Procedure:

A dry sample of about 500 g was prepared and weighed on a digital weighing balance. The sample was sieved through an already arranged set of sieves of different sizes. The samples retained on each sieve set were weighed and the value was recorded. The required calculations were performed and plotted accordingly.

Plate 1. Set of Sieve Sizes Arranged in Descending Order

2.3 Impact Value Test (IV)

Impact value test was carried out to determine the toughness of the aggregate used. This is shown in Plate 2.

Plate 2. Impact Value Test

Procedure:

Dry sample of aggregate passing 14 mm and retained on 10 mm BS sieve was used. An empty cylinder was weighed and recorded as (M_2). This sample was placed in three layers into the empty cylinder with each layer receiving 25 blows. Excess aggregate was removed from the top of the cup and the weight of the cylinder + sample was determined and recorded as (M_1). The compacted sample was placed in a mould directly on the base and placed in the impact machine. The placed sample was subjected to 25 blows. The crushed aggregate were sieved through a 2.36 mm sieve and the mass passing sample was weighed and recorded as (M_3). The weight of the compacted sample was recorded as (M_4).

The impact value was estimated using the expression in Equation (1).

$$IV\ (\%) = \frac{M4}{M3} * 100 \quad (1)$$

2.4 Specific Gravity Test (Gs)

Specific gravity is defined as the ratio of the weight in air of a given vol. of material or sample at a temperature to the weight in air of an equal volume of distilled water at the same temperature. This is used to determine various properties of aggregate.

Procedure:

The gas jar and the glass plate were weighed on a digital weighing balance (M_1). 300 g of dry sample was placed on the gas jar + plate and weighed as (M_2). Water was then added to the gas jar containing the sample and the entrapped air was expelled. Also, water was later added to the gas jar to the same level with the sample and recorded as (M_3). An empty gar jar was later filled with water and the weight was recorded as (M_4). The specific gravity was calculated using the expression in Equation (2):

$$Gs = \frac{M2 - M1}{(M4 - M1) - (M3 - M2)} \quad (2)$$

2.5 Compressive Strength Test

The quantities of cement, aggregates, and water were mixed together using the manual mixing method.

Procedure:

The values calculated in mix design were measured with the aid of a weighing balance. Slump test was carried out to determine the workability of the concrete prior to casting of 24 cubes of 150 mm × 150 mm × 150 mm. These concrete cubes were placed under laboratory condition of temperature for setting. The cubes were demoulded and immersed under water for curing for different curing periods (7 days, 14 days, 21 days, and 28 days). At the end of each curing period, 6 cubes were removed, air-dried and subject to a predetermined load to measure their compressive strength. These values were recorded, tabulated and presented in graphical forms to compare the strength at different curing periods. Some of the pictures captured during the compressive strength test are shown in Plates 3 & 4. The compressive strength is thus, estimated using the expression in Equation (3):

Plate 3. Compressive Testing Machine

Plate 4. Compressive Testing Machine during Crushing

$$Compressive\ Strength = \frac{crushingload\ (N)}{effectivearea\ (mm^2)} {}^{N}/_{mm^2} \quad (3)$$

3. Results and Discussions

This section highlights the results of the various laboratory tests and their discussions.

3.1 Material Quantity Estimation

Batching by weight method was used for all the 24 cubes produced for this study. Therefore, the results of the material quantities as estimated above are summarized in Table 1.

Table 1. Bill of Quantity Prepared for the Materials

S/N	Description	Quantity	Unit
1.	Quantity of cement in 1 m^3 of concrete	316	kg
2.	Volume of a concrete cube	0.003375	m^3
3.	Volume of 24 cubes concrete	0.0972	m^3
4.	Weight of cement required for a 24 cubes of concrete	31	kg
5.	Weight of water in 24 cubes	15	kg
6.	Weight of fine aggregate in 24 cubes	62	kg
7.	Weight of coarse aggregate in 24 cubes	124	kg

3.2 Sieve Analysis Test Result

The results of the sieve analysis test are divided into two parts; the part for the fine aggregate and the part for the natural gravel. The result of sieve analysis for the fine aggregate is tabulated in Table 2 while the particle size distribution curve is plotted in Figure 1. Similarly, for the natural gravel, the result of sieve analysis is tabulated in Table 3 while the particle size distribution curve is plotted in Figure 2.

Table 2. Sieve Analysis Test Result for the Fine Aggregate

Sieve size (mm)	wt. of Sample retained (g)	% Retained (%)	Cum. % retained	% Total Passing
4.75	6.00	1.20	1.20	98.24
2.36	16.00	3.20	4.40	95.04
1.18	70.00	14.00	18.40	81.04
0.60	186.00	37.20	55.60	43.84
0.30	170.00	34.00	89.60	9.84
0.15	44.00	8.80	98.40	1.04
0.08	4.20	0.84	99.24	0.20
Pan	1.00	0.20	99.44	

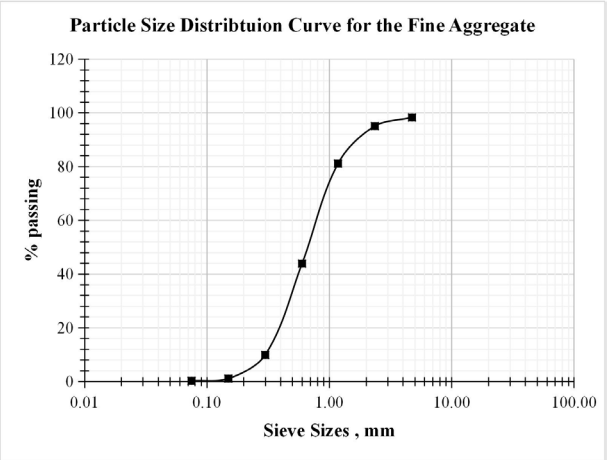

Figure 1. Particle Size Distribution Curve for the Fine Aggregate

Table 3. Sieve Analysis Test Result for the Natural Gravel

Sieve size (mm)	wt. of Sample retained (g)	% retained (%)	Cum % retained	% total Passing
20.00	150.00	15.00	15.00	47.70
13.20	39.00	3.90	18.90	43.80
10.00	200.00	20.00	38.90	23.80
4.75	152.00	15.20	54.10	8.60
2.36	73.00	7.30	61.40	1.30
0.60	12.00	1.20	62.60	0.10
0.30	1.00	0.10	62.70	0.00
Pan	0.10	0.20		

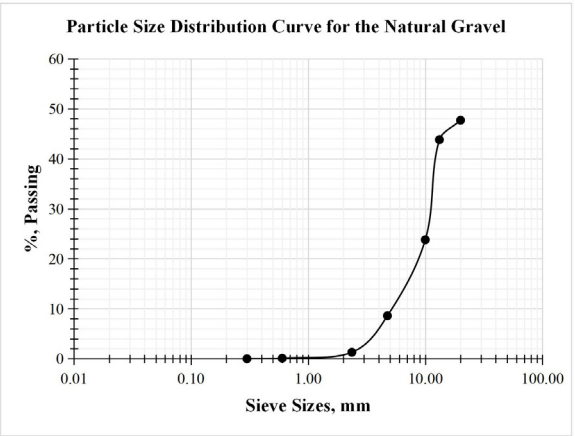

Figure 2. Particle Size Distribution Curve for the Natural Gravel

Coefficient of Curvature Determination

$$Cc = \frac{D30^2}{D60 * D10}$$

$$Cc = \frac{0.5^2}{0.8*0.3} = 1.04, \text{ approx. } 1$$

Coefficient of Uniformity Determination

$$Cu = \frac{D60}{D10}$$

$$Cu = \frac{0.8}{0.3} = 2.7 \ < 4.0$$

Thus, both the coefficient of curvature and coefficient of uniformity are approximately 1, it revealed that the fine aggregate material used is **UNIFORMLY GRADED SOIL**.

Coefficient of Curvature Determination

$$Cc = \frac{D30^2}{D60 * D10}$$

$$Cc = \frac{11^2}{70*5} = 0.35, < 1$$

Coefficient of Uniformity Determination

$$Cu = \frac{D60}{D10}$$

$$Cu = \frac{70}{5} = 14, \ > 4.0$$

Thus, both the coefficient of curvature and coefficient of uniformity are approximately 1.0, it revealed that the fine aggregate material used is **WELL GRADED GRAVEL**.

3.3 Impact Value Test Result

The result of Impact Value Test is tabulated in Table 4 while the bar chart showing the comparison between the two experimental trials is plotted in Figure 3. From Figure 3, it can be concluded that the results are relatively closed with each other. The average impact value for the natural gravel is estimated as 38.6.

Table 4. Impact Value Test for the Natural Gravel

Experimental trial	A	B
wt of mould + comp. sample (m_1)	1140.4	1145.2
wt of mould (m_2)	720.0	720.0
wt of comp. sample (m_1-m_2)	420.4	425.2
wt of fraction passing 2.36 mm sieve (m_4)	158.5	168.0
Impact Value = (m_4/m_3)*100	37.7	39.5
IV	**38.6**	

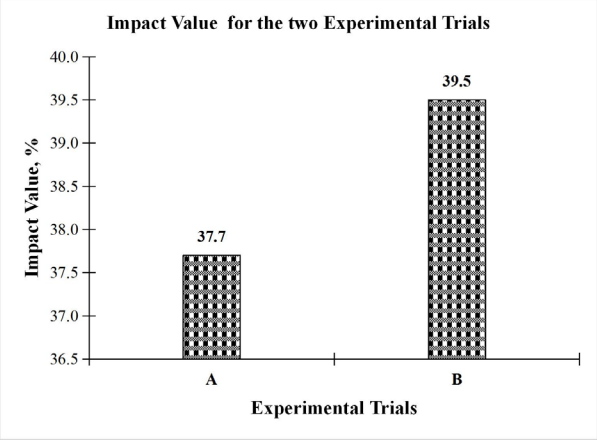

Figure 3. Impact Values for the two Experimental Trials

3.4 Specific Gravity Test Result

The result of Specific Gravity Test is tabulated in Table 5 while the bar chart showing the comparison between the specific gravity values for the fine and natural gravel aggregates are plotted in Figure 4. From Figure 4, it can be concluded that the specific gravity for sharp sand is higher than that for natural gravel. The average specific gravity for the natural gravel and fine aggregates is estimated as 2.62 and 2.64 respectively.

Table 5. Specific Gravity Test Results

Aggregate Type	Gravel		Sharp Sand	
Exp. Trials	**A**	**B**	**A**	**B**
wt of gas jar (m_1), (g)	102.20	101.10	103.50	103.50
wt of gas jar + plate + sample (m_2)	302.50	302.00	303.50	303.50
wt of gas jar + plate (m_3)	533.00	533.50	535.50	534.70
wt of gas jar + plate + water (m_4)	408.50	409.80	410.80	410.20
(m_2-m_1)	200.30	200.90	200.00	200.00
(m_4-m_1)-(m_3-m_2)	75.80	77.20	75.30	75.50
Specific Gravity (Gs) = (m_2-m_1)/[(m_4-m_1)-(m_3-m_2)	**2.60**	**2.60**	**2.65**	**2.64**
Average Gs	**2.62**		**2.64**	

3.5 Bulk Density Test Result

The bulk density test results for the fine aggregate and coarse aggregate are tabulated in Tables 6 and 7 respectively. A bar chart showing the comparison between the bulk density values for the fine and natural gravel

aggregates is plotted in Figure 5 for the two test types (loose and compacted).

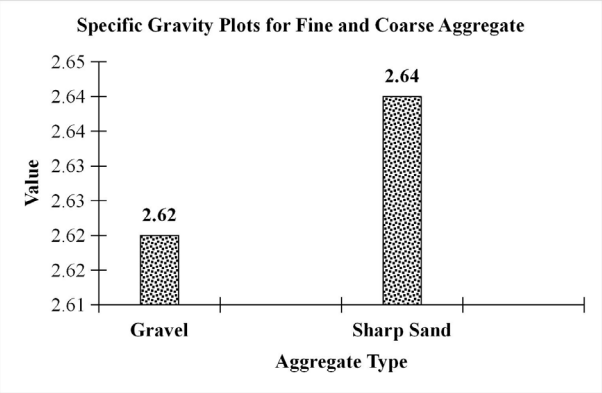

Figure 4. Specific Gravity Plots for both fine and coarse aggregates

Table 6. Bulk Density Test Results for Fine Aggregate

Sample	Fine Aggregate		Fine Aggregate	
Test Type	**Loose**		**Compacted**	
Exp. Trials	**A**	**B**	**A**	**B**
wt of comp. sample + mould (W_1) kg	0.758	0.765	0.81	0.803
wt of mould (W2) kg	0.025	0.025	0.025	0.025
wt of comp. sample (W_1 -W_2) kg	0.733	0.74	0.785	0.778
Volume of mould (V) (m^3)	0.000535	0.000535	0.000535	0.000535
Bulk density = [(W1-W^2)/V]	1370.1	1383.2	1467.3	1454.2
Avg. Bulk Density	**1376.65**		**1460.75**	

Table 7. Bulk Density Test Results for Natural Gravel

Sample	Natural Gravel		Natural Gravel	
Test Type	**Loose**		**Compacted**	
Exp. Trials	**A**	**B**	**A**	**B**
wt of comp. sample + mould (W_1) kg	0.762	0.758	0.858	0.863
wt of mould (W_2) kg	0.027	0.027	0.028	0.028
wt of comp. sample (W_1-W_2) kg	0.735	0.731	0.83	0.835
Vol. of mould (V) (m^3)	0.000535	0.000535	0.000535	0.000535
Bulk density = [(W_1-W_2)/V]	1373.8	1366.4	1551.4	1560.7
Avg. Bulk Density	**1370.1**		**1556.05**	

It can be noted the natural gravel bulk density is higher than that for the fine aggregate when the compacted test type was used while the reverse is the case for when the loose test type was used.

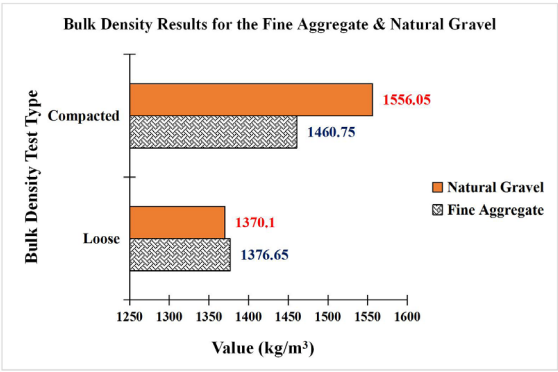

Figure 5. Bulk Density Plots for the Natural Gravel & Fine Aggregate

3.6 Slump/Compacting Factor Determination

The slump and compacting factor for both the dry and pre-saturated gravel are summarized in Table 8 and pictorially shown in Figures 6 and 7.

Table 8. Compressive Strength Result for the Pre-Saturated Coarse Aggregate

Mix Proportion		**1:2:4**	**w/c**	**0.48**
Sample	Aggregate Nature	Slump (mm)	Compaction Factor	Degree of work
	Dry	32	0.80	Low
	Pre-saturated	52	0.85	Medium

As shown in Figures 6 and 7, at the same conditions of mix-design ratio and water content, both the workability and the compaction factor for the pre-saturated aggregate are higher relatively to that for the natural dry aggregate. Thus, for the degree of work for the dry aggregate is low while that for the pre-saturated aggregate is medium.

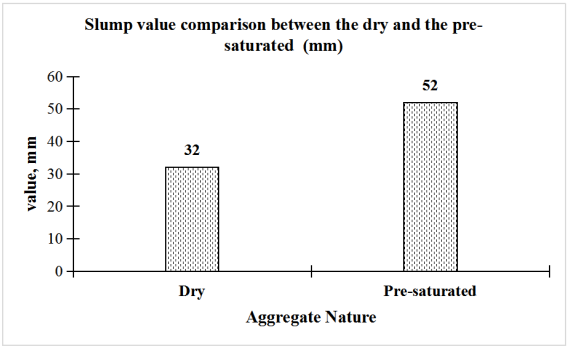

Figure 6. A Bar Chart Showing the Comparison between the Workability of the Dry and Pre-Saturated Coarse Concrete

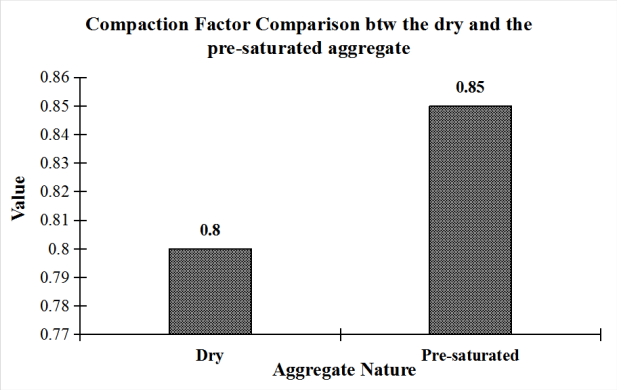

Figure 7. A Bar Chart Showing the Comparison between

3.7 Compressive Strength Result

The compressive strength test results for when the dry aggregate and pre-saturated aggregate were independently used for concrete are tabulated in Tables 9 and 10 respectively. A clustered bar chart comparing these strengths at different curing periods (i.e. 7 days, 14 days, 21 days, and 28 days) is shown in Figure 8.

Table 9. Compressive Strength Result for the Dry Aggregate

w/c		Area of mould (mm^2)		vol. of mould (mm^3)	
0.48		22500		3375000	
Age (days)	**Weight of cube (g)**	**Density of cube (g/mm^3)**	**Load at Failure (kN)**	**Comp. Strength (N/mm^2)**	**Avg. Strength (N/mm^2)**
7	8200	0.0024	385	17.20	**16.91**
	8140	0.0024	329	15.80	
	8140	0.0024	389	17.75	
14	8160	0.0024	400	18.15	**18.48**
	8120	0.0024	390	19.80	
	8150	0.0024	410	17.50	
21	8140	0.0024	450	20.20	**20.36**
	8160	0.0024	470	20.00	
	8200	0.0024	490	20.90	
28	8180	0.0024	600	26.50	**26.60**
	8140	0.0024	590	26.50	
	8100	0.0024	600	26.85	

Table 10. Compressive Strength Result for the Pre-Saturated Coarse Aggregate

w/c		Area of mould (mm^2)		vol. of mould (mm^3)	
0.48		22500		3375000	
Age (days)	**Weight of cube (g)**	**Density of cube (g/mm^3)**	**Load at Failure (kN)**	**Comp. Strength (N/mm^2)**	**Avg. Strength (N/mm^2)**
7	8170	0.0024	350	15.50	**15.08**
	8200	0.0024	340	14.75	
	8170	0.0024	320	15.00	
14	8150	0.0024	290	17.11	**17.45**
	8200	0.0024	300	18.00	
	8100	0.0024	425	17.25	
21	8200	0.0024	300	18.11	**18.45**
	8150	0.0024	290	19.00	
	8000	0.0024	270	18.25	
28	8000	0.0024	390	17.25	**19.05**
	8150	0.0024	400	18.95	
	8100	0.0024	329	20.95	

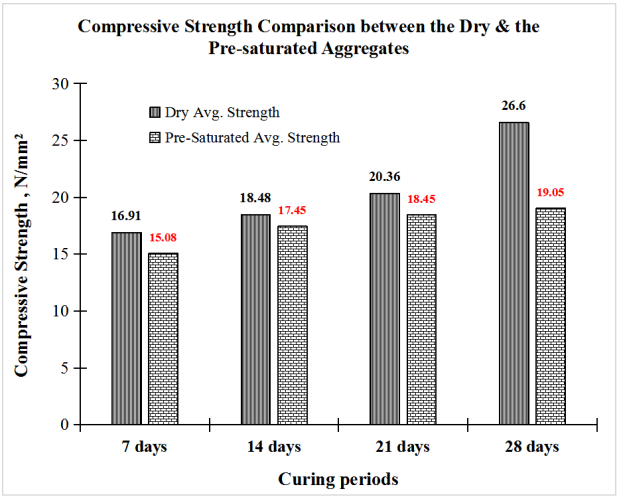

Figure 8. A Clustered Bar Chart Showing the Comparison between the Compressive Strengths of Dry and Pre-Saturated Coarse Aggregate

From Figure 8, it can be inferred that the compressive strengths at different curing periods for the pre-saturated aggregates were lower than those recorded at different curing periods for the dry aggregate. Thus, pre-saturation of aggregate has a negative impact on the strength of the concrete.

Table 11. Compressive Strength Result Summary

Age (days)	Dry Avg. Strength (N/mm^2)	Pre-Saturated Avg. Strength (N/mm^2)	Change in Strength (N/mm^2)	% Increment
7 days	16.91	15.08	1.83	10.8
14 days	18.48	17.45	1.03	5.6
21 days	20.36	18.45	1.91	9.4
28 days	26.60	19.05	7.55	28.4

4. Conclusions

It can be concluded that the bulk density of the dry gravel is higher than that for the fine aggregate when the compacted test type was used while the reverse is the case for when the loose test type was used. Also, the average specific gravity for the natural gravel and fine aggregates are estimated as 2.62 and 2.64 respectively. Also, the average impact value for the natural gravel is estimated at 38.6.

Also, the study concluded that at the same conditions of mix-design ratio and water content, both the workability and the compaction factor for the pre-saturated aggregate are higher relatively to that for the natural dry aggregate. Thus, for the degree of work for the dry aggregate is low while that for the pre-saturated aggregate is medium.

Finally, it can be concluded that the compressive strengths at different curing periods for the pre-saturated aggregates were lower than those recorded at different curing periods for the dry aggregate. Thus, pre-saturation of aggregate has a negative impact on the strength of the concrete. This study, thus, recommends that the pre-saturated aggregate be avoided/treated as much as possible in concrete production because it has a negative impact on the compressive strength of the concrete. That is, it reduces the compressive strength at different curing periods.

Acknowledgment

The authors acknowledge the Lab Attendants, Institute of Technology, Kwara State Polytechnic, Ilorin, Nigeria, for providing us with the lab machinery used for this study.

Data Availability

The datasets analyzed during the current study are part of this submission

Funding

This research did not receive any specific grant from funding agencies in the public, commercial or not-for-profit sectors.

Conflict of Interest

The authors declare no competing interest in this research paper.

References

[1] Chenglong, Z., Yu, C., 2019. The effect of nano-SiO_2 on concrete properties: a review. Nanotechnology Reviews. 8, 562-572.

[2] Venkat Rao, N., Rajasekhar, M., Vijayalakshmi, K., et al., 2015. The future of civil engineering with the influence and impact of nanotechnology on properties of materials. 2nd International Conference on Nanomaterials and Technologies (CNT 2014).

[3] Hansen, T.C., 1992. Recycled aggregates and recycled aggregate concrete, recycling of demolished concrete and masonry. International Union of Laboratories and Experts in Construction Materials, Systems and Structures. pp. 6.

[4] Oliveira, M.B.D., Vazquez, E., 1996. The influence of retained moisture in aggregates from recycling on the properties of new hardened concrete. Waste Management. 16(1-3), 113-117.

[5] Poon, C.S., Shui, Z.H., Lam, L., et al., 2004. Influence of moisture states of natural and recycled aggregates on the slump and compressive strength of concrete. Cement and Concrete Research. 34(1), 31-36.

[6] Czarnecki, L., 2013. Sustainable Concrete; Is Nanotechnology the future of concrete polymer composites? Advanced Materials Research. 687, 3-11.

[7] Feng, Y., Su, Y., Lu, N., et al., 2019. Meta Concrete: Exploring Novel Functionality of Concrete Using Nanotechnology. Engineered Science. 8, 1-10.

[8] Asokan, P., Mohini, S., Shyam, A.R., 2007. Solid wastes generation in India and their recycling potential in building materials. Building and Environment. 42, 2311-2320.

[9] Letelier, V., Ortega, J.M., Tarela, E., et al., 2018. Mechanical performance of eco-friendly concretes with volcanic powder and recycled concrete aggregates. Sustainability. 10, 30-36.

[10] Uzzal, H.Md., Rongjin, C., Thomas Ng, S., et al., 2020. Sustainable natural pozzolana concrete - A comparative study on its environmental performance against concretes with other industrial by-products. Construction and Building Materials. pp. 1-10.

[11] Lius, F., de Brito, J., Barra, M., 2011. Influence of

the pre-saturation of recycled coarse concrete aggregates on concrete properties. Magazine of Concrete Research. 63(B), 617-627.

[12] Pierre-Claude, A., 2000. Cements of yesterday and today: Concrete of tomorrow. Cement and Concrete Research. 30(9), 1349-1359.

[13] Cartuxo, F., de Brito, J., Evangelista, L., et al., 2015. Rheological behaviour of concrete made with fine recycled concrete aggregates - Influence of the superplasticizer. Construction and Building Materials. 89, 38-47.

[14] Chau-Khun, M., Abdullah, Z.A., Wahid, O., 2018. Structural and material performance of geopolymer concrete: A review. Construction and Building Materials. 186, 90-102.

[15] Rodrı ´guez-Robles, D., Garcı ´a-Gonza´lez, J., Juan-Valde´s, A., et al., 2015. Effect of mixed recycled aggregates on mechanical properties of recycled concrete. Magazine of Concrete Research. 67(5), 247-256.

[16] Tam, V.W.Y., Gao, X.F., Tam, C.M., 2005. Microstructural analysis of recycled aggregate concrete produced from two-stage mixing approach. Cement and Concrete Research. 35(6), 1195-1203.

[17] Etxeberria, M., Va´zquez, E., Marı, A., et al., 2007. Influence of the amount of recycled coarse aggregates and production process on properties of recycled aggregate concrete. Cement and Concrete Research. 37(5), 735-742.

[18] Lima, J., 1999. Proposition of guidelines for production and standardization of construction and demolition waste and of its application in mortars and concrete (in portuguese) Masters dissertation in Architecture and Urbanism. School of Engineering of Sao Carlos of the University of Sao Paulo, Sao Carlos.

BILINGUAL PUBLISHING CO.
Pioneer of Global Academics Since 1984

Journal of Building Material Science
https://ojs.bilpublishing.com/index.php/jbms

ARTICLE

Potentials of Balanite Endocarp Pod Ash as a Cement Replacement Material

Hassan Waziri Olumide Olubajo*

Chemical Engineering Department, Abubakar Tafawa Balewa University, Bauchi, Bauchi State, 740102, Nigeria

ARTICLE INFO

Article history
Received: 16 June 2022
Revised: 11 July 2022
Accepted: 16 July 2022
Published Online: 20 July 2022

Keywords:
Balanite endocarp pod ash
Consistence
Setting time
Cement replacement
Curing days

ABSTRACT

The exponential growth of agricultural wastes such as Balanite seed pod has resulted in waste management issues and finding alternatives through waste recycling is an interesting area of research. Balanite seed pods were collected in Yobe state, washed, dried, crushed. Balanite endocarp pod ash (BEPA) was calcined at 600 °C for 3 hours in a muffle furnace and the biomass was characterized with X-ray fluorescence spectrometer to determine its chemical composition. The analysis showed that the ash composed of silica, alumina and ferric oxide (74.24 wt.%) indicated a strong pozzolan based on American Standard. The BEPA possessed a high loss on ignition of 8.24 wt.% owing to the presence of unburnt carbon in the ash. The ash obtained was sieved with 75 μm sieve and cement was replaced with ash between 2.5 wt.% ~ 12.5 wt.% at interval of 2.5 wt.% to assess its impact on cement properties such as setting time, consistence, mortar strength and water absorption. Results showed that as percentage replacement increases, the water absorption increased while the mortar strength diminished whereas as the curing days progressed its strength improved despite clinker diminution due to cement hydration. 60 days strength for below 10 wt.% BEPA cement blend produced enhanced strength compared with control which is evidence of slow pozzolanic reactions. The optimum percentage replacement with BEPA was obtained at 7.5 wt.% replacement beyond which significantly affected the cement properties especially its strength. It could be agreed that BEPA has potentials to be considered and employed as a cement replacement material.

1. Introduction

Balanite Aegyptiaca (laloub) is a spiny semi- evergreen shrub from the family tree of the Zygophyllaceae spanning about 12 m high producing yellow date-like fruits [1]. Balanite Aegyptiaca is also referred to as desert date, fondly known as Laloub in Arabic, Aduwa in Hausa, Hingota in Hindi and Zagum Mitzi in Hebrew. The fruit yield of a mature tree bears as much as 10,000 fruits per annum. A single fruit comprises of (5%-9%) epicarp,

*Corresponding Author:
Olumide Olubajo,
Chemical Engineering Department, Abubakar Tafawa Balewa University, Bauchi, Bauchi State, 740102, Nigeria;
Email: ooolubajo@atbu.edu.ng

DOI: https://doi.org/10.30564/jbms.v4i1.4800

(28%-33%) mesocarp or pulp, (49%-54%) endocarp, and (8%-12%) kernel with oil content of B. Aegyptiaca seed approaches 50% [2-4]. The fruit is a plum like drupe, pubescent when green becoming yellowish and glabrous after ripening [5]. The fruit possesses four main parts namely the epicarp, mesocarp, endocarp and the kernel. The fruit when ripen is a drupe possessing brownish to reddish thin epicarp, a dark brown, fleshy mesocarp and a thick endocarp with the seed [6-8]. The whole fruit yields half of the woody shells which are hard, dense and highly combustible. The Balanite fruits is considered a resilient evergreen tree beneficial to mankind for centuries as well as one of the oldest fruits which dates back to the era of Pharaoh's tombs around the 12th dynasty in ancient Egypt. It is an underutilized tree which possesses numerous uses and its surprising that it has been exploited beyond its potential use. The tree provides many uses ranging from feedstock for livestock to medicinal purposes. They make good fuel as well as good charcoal and particle board [9]. Balanite A. is one of the widely distributed woody plants in many African countries including Nigeria especially adapting in semi-arid and arid regions of tropical Africa and its subspecies are reported to be found only in India [7,10-12]. Most literature explores the extraction of oil from the seed, use of Balanite pod as a light coarse aggregate in construction [13,14]. The purpose of this research work investigates the possibility of the calcined endocarp of the Balanite Aegyptiaca fruit employed as a cement replacement material and the impact on the properties of cement.

The problem of disposal of agricultural wastes has begun to give great concern globally which could be detrimental to human health. Similarly, due to high cost of cement production coupled with released CO_2 emission tends to affect the greenhouse resulting in global warming. Other issues include the high cost of electricity mounting pressure on the use of wood resources stemming from the high energy demand from the growing population. Thus, forcing researchers to seek for alternatives to prevent over harvesting and deforestation [15]. Thus, there is a need to employ the use of biomass is imperative from other sources other than wood such as endocarp of balanite pod. The energy intensiveness of the cement industry coupled with the need to produce cement blends with better technical properties has provided the opportunity to replace endocarp of balanite pod with wood which is readily available and possess a high calorific value which could be employed as fuels and the resultant ash can serve as a cement replacement material.

Researchers have already been expanding innovative technologies to achieve sustainable raw materials in the construction and building industry. One of the ways through the use of agricultural waste can be utilized and employed as construction materials. Balanite seeds can be considered as a renewable source and possesses the potential to be employed as a cement replacement material in the building industry in Nigeria. It is in this light, that this study investigates the potential of BEPA as cement replacement material in the construction industry. Mangi et al. [16] stated that the concrete industry consumes a huge chunk of natural aggregates and suggested that the potential of using date palm seed for structural lightweight concrete as well as cheap alternative to gravels, but its durability as an aggregate was called in to question due to the inability to withstand exposure to marine or hydraulic structures [17-21] also proved that the utilization of ash-based cementitious materials is not only environment-friendly but possessed more or less same or better properties compared to conventional concretes/mortars. Previous works have studied the use of other pods like date palm pod ash, palm kernel seed ash, locust bean pod ash etc. as cement replacement material with various success but no work has investigated the use of the ash of endocarp of Balanite pod as a cement replacement material as well as the impact on cement properties. Thus, there was a need to also explore the optimum dosage of these local material which is readily available.

The quality of the cement was blended between 0 -12.5 wt.% at interval of 2.5 wt.% were assessed based on various properties such as consistency, setting time, mortar compressive strength, water absorption according to ASTM standards. This research tries to understand the chemical composition of the BEPA and the impact of replacement of cement with the ash on the cement quality and finally determination of the optimal cement replacement for the mortar strength as well as the water absorption rate.

2. Materials and Method

The materials employed for this study are Portland limestone cement was obtained from Dangote Plc which belongs to class CEM II 42.5R A-L while Balanite seed which was sourced at Damaturu market in Yobe State which was calcined to obtain BEPA. Standard sand was obtained from sieving sand into 3 categories comprising between less than 2 mm IS sieve and residue of 90 microns IS sieve. Sieve ranges include less than 2 mm but greater than 1 mm (33.33%), less than 1mm but greater than 600 microns (33.33%) and less than 600 microns but greater than 90 microns (33.33%). The specific gravities of the 3 divisions of the sand were 2.77, 2.67 and 2.59 respectively. Table 1 summarizes the chemical

composition of Portland limestone cement and BEPA using X-ray Spectrometer. The standard Bogue calculation is significantly useful in determination of the proportion of the four minerals in Portland cement:

$$C3S = 4.0710CaO - 7.6024SiO2 - 1.4297Fe2O3 - 6.7187Al2O3 \quad (1)$$

$$C2S = 8.6024SiO2 + 1.0785Fe2O3 + 5.0683Al2O3 - 3.0710CaO \quad (2)$$

$$C3A = 2.6504Al2O3 - 1.6920Fe2O3 \quad (3)$$

$$C4AF = 3.0432Fe2O3 \quad (4)$$

Table 1. Chemical composition of Portland limestone cement and Balanite endocarp pod ash

Compound	PLC	BEPA
SiO_2	13.39	70.26
Al_2O_3	4.20	1.12
Fe_2O_3	1.95	2.86
CaO	42.14	11.94
P_2O_5	0.18	-
K_2O	0.63	3.92
TiO_2	0.19	0.00
MgO	0.74	0.74
MnO	0.10	-
Na_2O	0.09	0.34
SO_3	1.03	0.38
Cl	0	0.03
LOI	34.67	8.42
Total	47.49	100.00
SiO_2 +Al_2O_3 +Fe_2O_3	35.26	74.24
C_3S	38.75	-
C_2S	9.16	-
C_3A	7.83	-
C_4AF	5.93	-

Balanite seeds were collected from Damaturu, Yobe State, were first open- dried under the sun for a longer period. The dried Balanite pods were then crushed to separate the seeds from the pods and the pods (endocarp) was then calcined with a furnace at 600 °C for 3 hours and the resultant ash was ground to powder and sieved with 90-micron sieve. Characterization of the BEPA was conducted using X-ray Fluorescence spectrometer to determine its chemical composition. Table 2 presents the physical properties of the fine aggregate or standard sand employed in mortar preparation.

Table 2. Physical properties of Standard sand

Parameter	Standard sand
Appearance	Brownish solid
Specific gravity	2.67
LOI	0.27

The experimental matrix for the determination of the physical and mechanical properties of Portland limestone cement and BEPA cement blends are presented in Table 3.

Table 3. Experimental matrix for BEPA cement blend physicomechnical properties

S/No	Cement Blends	PLC wt.%	BEPA wt.%
1	PLC	100	0.0
2	2.5BEPA	97.5	2.5
3	5BEPA	95	5.0
4	7.5QBEPA	92.5	7.5
5	10BEPA	90	10.0
6	12.5BEPA	87.5	12.5

Figure 1 depicts the washed Balanite seed that was open dried while Figure 2 shows the calcination of the separated Balanite endocarp pod in a muffle furnace. Figure 3 shows the BEPA obtained from calcination in the muffle furnace at 600 °C for 3 hours.

Figure 1. Washed balanite seed

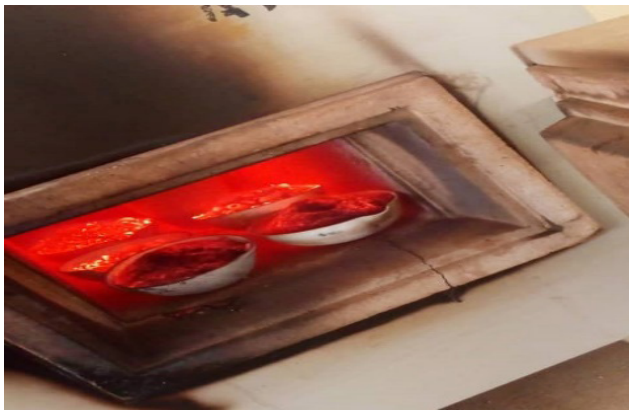

Figure 2. Calcination of balanite pod

Figure 3. Balanite endocarp pod ash

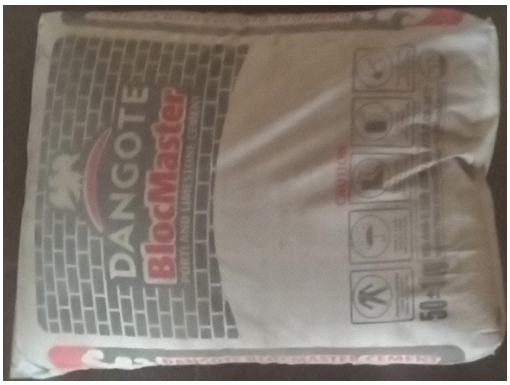

Figure 4. Portland limestone cement

The Vicat method was specified by the ASTM, C-618 [22], was used to determine the standard consistency of blended cement paste. Three hundred grams (300 g) of cement blends was mixed with water to form paste which were gauged until the resistance to penetration of a plunger reaches between 5 mm - 7 mm from the bottom of the Vicat mould. The ratio of the water required to the weight of cement which was expressed as a percentage was taken as the standard consistency of the cement.

$$Standard\ Consistency\ (\%) = \frac{Weight\ of\ water\ added}{Weight\ of\ cementitious\ material} \times 100 \quad (5)$$

The Vicat method was also employed to determine consistence and both setting times specified by ASTM C 187 [23], ASTM C 191 [24] respectively. The water consistence of the various cement blends obtained were then used to determine the initial setting time of the various cement blends and their pastes were gauged into the Vicat mould. The blended cement paste was placed under the Vicat apparatus with the needle provided for the initial setting time determination. The needle was then lowered gently into the contact with the surface of the test block and quickly released and allowed to sink in. This process was repeated until the needle did not penetrate beyond a point approximately 4 mm from the bottom of the mould. The period elapsing between the time when the water was added to the cement and the time at which the needle ceased to pierce beyond 4 mm from the bottom of the test block was noted as the initial setting time T_2 - T_1. The needle for initial setting time was replaced with annular attachment to determine the final setting time. When the needle did not make an impression on the needle was gently applied on the surface of the test block. The final setting time is the time from when water was added to the cement blend and when the needle ceased to pierce the test block T_3 - T_1. Where T_1 refers to the time at which water was first added to the cementitious material, T_2 refers to the time when the needle fails to penetrate 5 mm - 7 mm from the bottom of the Vicat mould while T_3 refers to the time when the needle made an impression but the attachment fails to do so.

The water absorption test was conducted on mortars according to BS 1881-122 [25]. Triplicate of mortar cubes after casting were immersed in water for 28 days curing. These specimens were then removed from the curing tank and oven dried for 24 hours at the temperature 85 °C until the mass became constant and again weighed. The weight was noted as the dry weight of the specimen. After that the specimen was kept in water at 85 °C for 24 hours. Then this weight was noted as the dry weight of the specimen.

$$\%\ Water\ Absorpion = \frac{Weight\ wet - Dry\ weight}{Dry\ weight} \times 100 \quad (6)$$

The compressive strength tests were conducted on moulds of 50 mm mortar cube in accordance with ASTM C 109 [26]. A mix ratio of water, cement and standard sand (1:2:4) was adopted to obtain mortars in which the cement was gradually replaced with BEPA between 2.5 wt.% - 12.5 wt.% at interval of 2.5 wt.% at curing age of the specimen at 3, 7, 28 and 60 days respectively. The mortars were homogeneously mixed and placed in moulds and set on a metal slab and bolts on the moulds were fasten with spanner. The cubes were prepared in triplicates at an average temperature of 20 °C and relative humidity of less than 50%. The assembled moulds were then placed in a vibrating machine and securely held in place while filled with the mortars. The moulds were then vibrated with the aid of a jolting machine for 2 minutes, followed by the specimen being were covered with an impervious sheet to avoid evaporation and were cured at room temperature for 24 hours. The cubes were then demoulded after 24 hours and were designated by codes for identification. The mortar cubes were then cured in a tank with distilled water at various ages of 3, 7, 28 and 60 days. The compressive strength test for the mortar was obtained using Tonic Technic compression and machine for triplicates of the cubes which were crushed to

obtain an average strength for the various cement blends.

$$Compressive\ strength = \frac{Load}{Cross\ sectional\ area} \quad (7)$$

3. Results and Discussion

From the chemical analysis, Portland limestone cement is an innovative cement that contains between 5 wt.% - 15 wt.% well ground limestone. The percentage of lime and silica were found to be lower compared to the specification ranges for ordinary Portland cement whereas, the other oxides all fall within the range as reported by British standard BS 12 [27]. Based on the X-ray Fluorescence result obtained, it was clearly seen that BEPA significant silica present in its composition and thus can serve as a suitable cement replacement. It was also observed that BEPA obtained from calcination of the endocarp of Balanite seed at 600 °C for 2 hours consisted of more than 70 wt.% of $SiO_2 + Al_2O_3 + Fe_2O_3$ (74.24 wt. %) while CaO content was 11.94 wt.% which met class C with CaO content > 10%, hence the ash satisfies as a pozzolan according to ASTM C 618, thus possessing both self-binding and pozzolanic properties [22,31]. The loss on ignition of BEPA was 8.42% indicating a high degree of unburnt carbon of ash [28,29] which is also responsible for increase in the water requirement due to the high porosity of the BEPA particle resulting in mixture segregation which agrees with Freeman et al. [30], Kaya [31]; Olubajo and Osha [32], Olubajo et al. [33]. Table 4 indicates the effect of replacing Portland limestone cement with BEPA at replacement intervals of 2.5 wt.% from 2.5 wt.% - 12.5 wt.% on consistence, initial and final setting time and water absorption of mortars.

Table 4. Influence of BEPA on the consistence and setting times and water absorption of cement bends

BEPA content (wt.%)	Consistency (%)	Water demand (mL)	Initial Setting time (min)	Final setting time (mm)	Water Absorption (%)
0.0	30.0	135.0	147	177	7.10
2.5	31.4	141.3	186	202	7.47
5.0	31.2	140.4	170	185	8.71
7.5	31.0	139.5	176	190	9.25
10.0	31.6	142.2	165	186	10.04
12.5	31.6	142.2	158	186	10.06

Figures 5 and 6 indicate the effect of BEPA content on the water absorption and consistence of BEPA - cement blend respectively. It could be observed from Figure 5 that as cement was gradually replaced with BEPA from 0 - 12.5 wt.% at 2.5 wt.% led to an increase in the rate of water absorption. This increase in the water absorption value observed could be attributed to high loss of ignition owing to the high carbon content present in the BEPA. Portland limestone cement produced the least water absorption of 7.1% as against 10.06% for 12.5 wt.% with BEPA which increased by 42.5% indicating that the ash content significantly affects the water absorption of cement blended with BEPA. According to Olubajo [34], Olubajo & Odey [35]; Sprung & Siebel [36] suggested that the particle size distribution of the ash could influence the strength which in turn affects the rate of water absorption of blended cement mortars. An increase in the water absorption at 28 days was experienced as the cement replacement level with BEPA was increased from 2.5 wt.% - 12.5 wt.% which was contrary to Chai et al. [37] findings. This increase in the water absorption could be linked with increase in the water demand, retardation of its setting times and finally lower strengths. The significant particle pores in the mortars could be linked with the high BEPA content culminating in formation of less dense structure thus allowing water to penetrate easily. Chai et al. [37] also suggested that the relationship between the rate of water absorption was inversely proportional to the mortar compressive strength which agrees with this work with an increase in the rate of water absorption and a reduction in the 28 days strength as the cement replacement level was increased.

Similar trend was observed for BEPA-cement blends requiring more water to attain consistence in comparison with control and cement blended with other ashes such as locust bean pod ash [29], sugarcane bagasse ash [33], coal bottom ash [32,38]. The impact of the BEPA on the water requirement increased from 31% - 31.6% (90 mL - 95 mL) as the cement replacement was increased between 0 - 12.5 wt.%. This increase in the water consistence could be attributed to the high loss on ignition of the BEPA arising from carbon content present in the BEPA incorporated into the cement blend. Thus, inclusion of BEPA into the cement matrix resulted in a higher water consistence compared with control.

Table 5 tabulates the mortar strength of cement blends as a function of the cement replaced with BEPA content as well as their percentage strength gain in comparison with control strength while Figures 8 and 9 depict the effect of cement replacement and curing age on the mortar compressive strength of BEPA-cement blends. For 3 days strength, it could be seen that as the cement replacement level was gradually increased, the various cement blends produced a better strength gain compared with control by 7.80% and 9.85% for 2.5 wt.% and 5 wt.% cement replacement respectively. Whereas, beyond 5 wt.% cement replacement produced lower strengths in comparison with control with strength reduction for

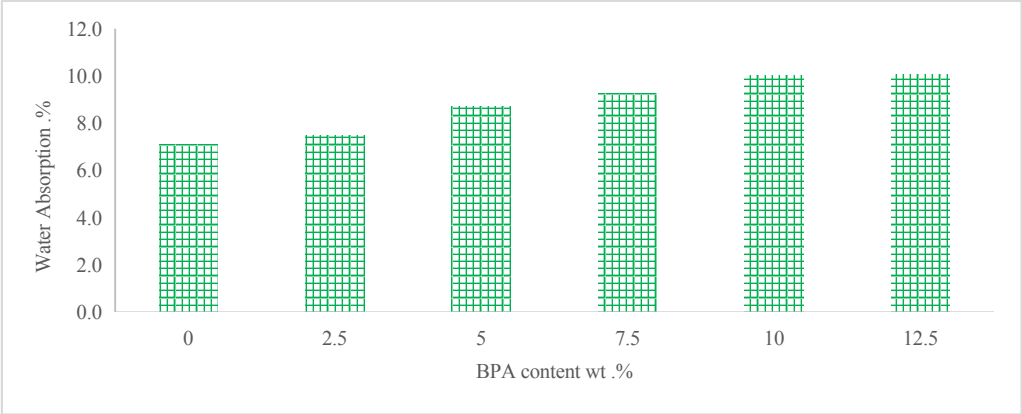

Figure 5. Effect of BEPA content on Water Absorption of cement blends

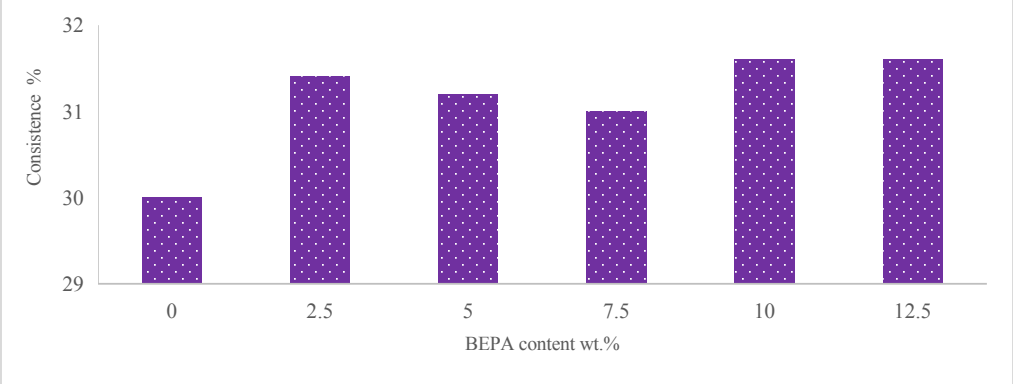

Figure 6. Effect of BEPA content on water consistence of cement blends

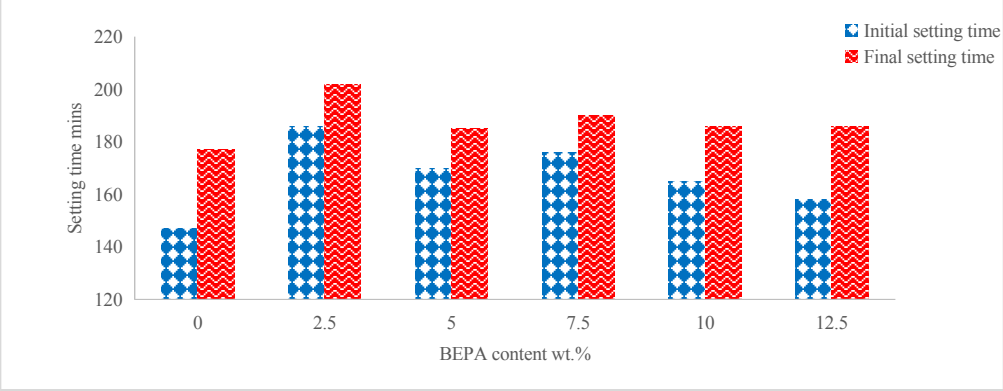

Figure 7. Effect of BEPA content on Setting times of cement blends

7.5 wt.% (15.34%), 10 wt.% (12.99%) and 12.5 wt.% (23.83%) respectively. The increase in the strength could be linked with pozzolanic activity which occurs despite the reduction in the tricalcium silicate/dicalcium silicate (C_3S/C_2S) content, thus resulting in slight increase at lower cement replacement of BEPA. The C_2S, C_3S, are part of the four main minerals were obtained from standard bogue calculation to determine their approximate proportions which gives an idea of the quality of the clinker/cement. Whereas, at high cement replacement with BEPA produced lower 3 days strength as a result of diminution of clinker effect owing to significant reduction in the C_2S/C_3S content which is responsible for early strength.

The 7 days strengths experienced a decrease in its strength by 39.89% as cement was gradually replaced with BEPA whereas, the 28 days strength of BEPA-cement blends were lower than the control. This reduction

in strength at 7 and 28 days could be attributed to the diminution of the clinker content resulting in formation of limited CSH compared to control as reported by Olubajo and Osha [32]. Another reason for the lower strengths could be due to presence of the unburnt carbon in BEPA, resulting in higher water consistence, retarded setting times culminating in lower compressive strengths as the BEPA content was increased. It could be observed from Figure 8 that the 60 days strength of cement blended with 2.5 wt.% - 7.5 wt.% BEPA produced a better strength gain compared with control of 41.9 N/mm^2 as against 43.88 N/mm^2 (4.73%), 43.66 N/mm^2 (4.20%) and 42.30 N/mm^2 (0.95%). A reduction in the strength by 9.31% and 20.86% was observed for cement replacements for 10 wt.% and 12.5 wt.% respectively. The initial strength gain experienced between 2.5 wt.% - 7.5 wt.% BEPA could be linked with pozzolanic activity exhibited by the inclusion of BEPA content resulting in the production of CSH despite diminution of the clinker content which agrees with Olubajo et al. [39].

Figure 9 depicts the mortar compressive strength of various BEPA cement blends at various cement replacements as a function of curing age ranging from 3 days to 60 days. It indicated that the strength of blended mortars exhibited a direct relationship with the curing age as the hydration process progresses for various cement replacement. This is in agreement with Olubajo et al. [39] in which also experienced similar trends suggesting that despite diminution of the clinker content, apart from the hydration reaction taking place, slow pozzolanic reaction occurs between the excess lime and silica presence in the ash to produce more CSH, thus resulting in mortars developing excellent strength in comparison to control.

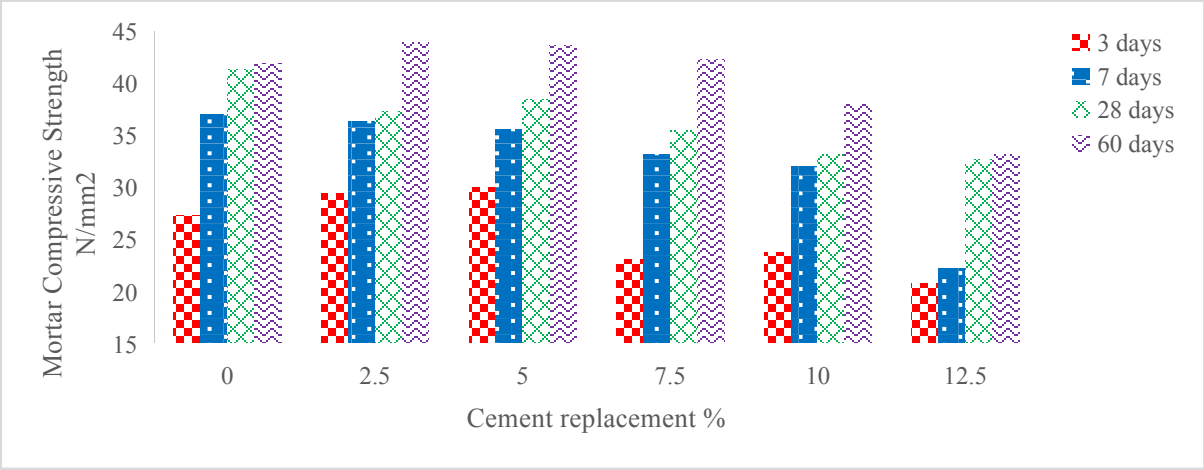

Figure 8. Effect of cement replacement on the mortar compressive strength of various cement blended BEPA and curing days

Table 5. Compressive Strength of mortar for various percentage replacements at different curing days

Cement replacement wt.%	Compressive Strength N/mm^2							
	3 days	Strength gain (%)	7 days	Strength gain (%)	28 days	Strength gain (%)	60 days	Strength gain (%)
0	27.32	100.00	37.05	100.00	41.3	100.00	41.9	100.00
2.5	29.45	107.80	36.32	98.03	37.3	90.31	43.88	104.73
5	30.01	109.85	35.55	95.95	38.49	93.20	43.66	104.20
7.5	23.13	84.66	33.17	89.53	35.52	86.00	42.3	100.95
10	23.77	87.01	32.01	86.40	33.2	80.39	38	90.69
12.5	20.81	76.17	22.27	60.11	32.72	79.23	33.16	79.14

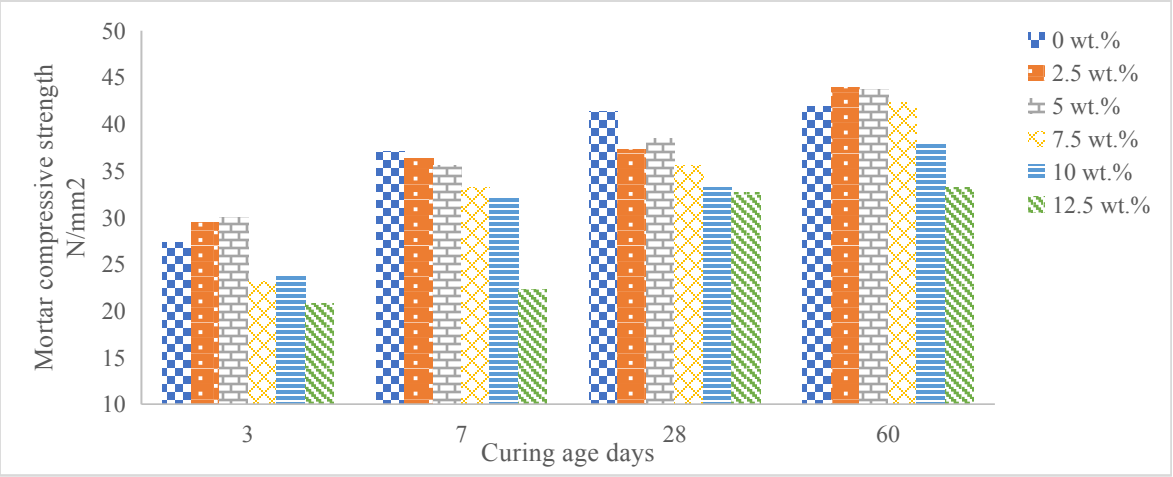

Figure 9. Effect of curing age on the mortar compressive strength of various cement blended BEPA at different cement replacements

4. Conclusions

From this study, it was concluded that BEPA are suitable to be employed as partial cement replacement as a construction material. The chemical composition of BEPA indicated majority of its content comprising of silica, alumina and ferric oxide up to 76 wt.% with CaO content more than 10 wt.%, thus classifying it as Class C pozzolanic material thus having self-binding properties along with pozzolanic properties. Results indicated that the percentage of BEPA should not exceed 7.5 wt.% for mortar compressive strength beyond which results in significant reduction in compressive strengths in comparison with control especially at 60 days. The water absorption of mortars blended with BEPA at 28 days experienced an increase as the replacement of cement with BEPA which was linked with increase in the BEPA content resulting in higher consistence and setting times. All BEPA cement blends experienced an increase in its strength as the curing days progressed. Cements blended up to 12.5 wt.% BEPA are recommended for application in general construction due to the fairly high C_3S content required for early strength.

Conflict of Interest

The authors declared that they have no conflict of interest.

Acknowledgments

The authors wish to appreciate Bua Cement Plc, Ashaka Cement Plc Nigeria, and Departments of Chemical and Civil Engineering of Abubakar Tafawa Balewa University, Bauchi Nigeria for providing infrastructure, facilities and their support to this research work.

References

[1] AI-Thobaiti, S.A., Zeid, I.M.A., 2018. Medicinal Properties of Desert Date Plants (Balanites Aegyptiaca) - An Overview. Global Journal of Pharmacology. 12(1), 01-12.

[2] Chapagain, B., Wiesman, Z., 2005. Variation in diosgenin level in seed kernels among different provenances of Balanites aegyptiaca Del (Zygophyllaceae) and its correlation with oil content. African Journal of Biotechnology. 4(11), 1209-1213.

[3] Chapagain, B.P., 2006. Characterization of Desert Date (Balanites Aegyptiaca) Saponins and Their Biological Activities; Ben-Gurion University of the Negev: Beer-Sheva, Israel.

[4] Okia, C.A., Kwetegyeka, J., Okiror, P., et al., 2013. Physico-chemical characteristics and fatty acid profile of desert date kernel oil. African Crop Science Journal. 21, 723-734.

[5] Arbonnier, M., 2004. Trees, shrubs and lianas of West Africa Dry Zones. CIRAD, MARCRAF Publishers. pp. 572.

[6] Eyog, M.O., Gandé, G.O., Dossou, B., 2000. Programme de ressources génétiques s en Afrique au sud du Sahara. IPGRI édition, Rome. pp. 243.

[7] Sagna, M.B., Diallo, A., Sarr, P.S., et al., 2014. Biochemical composition and nutritional value of Balanites aegyptiaca (L.) Del fruit pulps from Northern Ferlo in Senegal. African Journal of Biotechnology. 13(2), 336-342.

[8] Mohamed, A.M., Wolf, W., Spiess, W.E., 2002. Physical, morphological and chemical characteristics, oil

recovery and fatty acid composition of Balanites Aegyptiaca Del. kernels. Plant Foods Hum Nutr (Dordrecht, Netherlands). 57, 179-189.

[9] National Research Council, 2008. Lost Crops of Africa: Volume III, Fruits, Development, Security and Cooperation. The national Academies Press, Washington, D.C.

[10] Booth, F.E.M., Wickens, G.E., 1988. Non-timber uses of selected Arid zone trees and shrubs in Africa. FAO Conservation Guide. 19.

[11] Hall, J.B., Walker, H.D., 1991. Balanites Aegyptiaca: A monograph. School of Agriculture and Forest Sciences Publication Number 3. University of Wales.

[12] Chevallier, M.H., Vaillant, A., Bensaid, S., et al., 2004. Impact des pratiques humaines sur la conservation et la gestion in situ des ressources forestières: cas d'Acacia tortilis raddiana et de Balanites aegyptiaca. CSFD, Rapport du projet n°57, 68.

[13] Kau, K.A., Osakwe, C.E., Tikikus, K.S., 2019. The use of balanite seed for partial replacement as aggregate in lightweight concrete. Nigeria Journal of Engineering Science and Technology Research. 5(2), 90-95.

[14] Andi, S., Gufran, D.D., Muhammad, I.A., 2021. Investigation of the Effect of using Salak Seeds as Coarse Aggregate. Concrete Asian Journal of Applied Sciences. 9(3), 172-178.

[15] Sulaiman, C., Abdul-Rahim, A.S., Mohd-Shahwahid, H.O., et al., 2017. Wood fuel consumption, institutional quality, and forest degradation in sub-Saharan Africa: Evidence from a dynamic panel framework. Ecological Indicators. 74, 414-419.

[16] Mangi, S.A., Wan Ibrahim, M.H., Jamaluddin, N., et al., 2019. Short-term effects of sulphate and chloride on the concrete containing coal bottom ash as supplementary cementitious material. Environmental Science and Pollution Research. 22(2), 515-522.

[17] Akib, S.M., Bhuva, D., Pindoriya, D., 2018. Exploratory Study on Partial Replacement of Coarse Aggregate by Date Seed. pp. 2-6.

[18] Islam, M.M.U., Mo, K.H., Alengaram, U.J., et al., 2016. Mechanical and Fresh Properties of Sustainable Oil Palm Shell Lightweight Concrete Incorporating Palm Oil Fuel Ash. Journal of Cleaner Production. 115, 307-314.

[19] Mujah, D., 2016. Compressive Strength and Chloride Resistance of Grout containing Ground Palm Oil Fuel Ash. Journal of Cleaner Production. 112, 712-722.

[20] Ozerkan, N.G., Ahsan, B., Mansour, S., et al., 2013. Mechanical performance and durability of treated palm fiber reinforced mortars. International Journal of Sustainable Built Environment. 2, 131-142.

[21] Olubajo, O.O., Abdullahi, B., Osha, O.A., 2019. The potential of Orange Peel Ash as a Cement Replacement Material. Path of Science. 6(2), 1629-1635. Available on website link: http://www.pos.org.

[22] ASTM, 2008. C618-08a: Standard Specification for Coal Fly Ash and Raw or Calcined Natural Pozzolan for Use in Concrete. Annual Book of ASTM Standards.

[23] ASTM C 187, 2010. Standard test method for normal consistency of hydraulic cement. Annual Book of ASTM Standards.

[24] ASTM C191-19 - Standard Test Methods for Time of Setting of Hydraulic Cement by Vicat Needle. Annual Book of ASTM Standards.

[25] BS 1881:122, 2011. Method for Determination of Water Absorption.

[26] ASTM C 109, 2008. Standard test method for compressive strength of hydraulic cement mortars. Annual Book of ASTM Standards.

[27] British Standard Institution, 1996. BS 12: Specification for Portland Cement. British Standard Institution, London.

[28] Külaots, I., Hurt, R.H., Suuberg., E.M., 2004. Size distribution of unburned carbon in coal fly ash and its implications. Fuel. 83, 223-230.

[29] Olubajo, O.O., Osha, O.A., Abubakar, J., 2020. Setting Times of Portland Cement Blended with Locust Bean Pod and Eggshell Ashes, American Journal of Chemical Engineering. 8(5), 103-111. Available on website link: http://www.sciencepublishinggroup.com/j/ajche.
DOI: https://doi.org/10.11648/j.ajche.20200805.11

[30] Freeman, E., Gao, Y.M., Hurt, R., et al., 1996. Interactions of carbon containing fly ash with commercial air-entraining admixtures for concrete. Fuel. 76, 761-765.

[31] Kaya, A., 2010. A study on blended bottom ash cements MSc. Thesis, Middle East Technical University. 1-73.

[32] Olubajo, O.O., Osha, O.A., 2013. Influence of bottom ash and limestone powder on the properties of ternary cement and mortar. International Journal of Engineering Research and Technology. 12(7), 1201-1212. Available on website link: http://www.ijert.org.

[33] Olubajo, O.O., Nuuman, A., Nazif, L.S., 2020. The Effect of Sugarcane Bagasse Ash on the Properties of Portland Limestone Cement. American Journal of Construction and Building Materials. 4(2), 77-87. Available on website link: http://www.sciencepub-

lishinggroup.com/j/ajcbmm
DOI: https://doi.org/10.11648/j.ajcbm.20200402.15

[34] Olubajo, O.O., 2020. The Effect of Eggshell Powder and Saw Dust Ash on the physicomechnical properties of blended cement. American Journal of Construction and Building Materials. 4(2), 88-99. Available on website link: http://www.sciencepublishing group.com/j/ajcbm
DOI: https://doi.org/10.11648/j.ajcbm.20200402.15

[35] Olubajo, O.O., Odey, O.A., 2021. The Effect of Eggshell Powder and Glass powder on the Mortar compressive strength of Ternary Cement ICOST conference 2020. Proceeding of International Conference 2020 University of Technologi Malaysia. Available on website link: http://www.Icost2020.utm. edu.my. Lecture Notes in Mechanical Engineering- Springer.

[36] Sprung, S., Siebel, E., 1991. Assessment of the suitability of limestone for producing Portland limestone cement. ZKG International, Edition B. 44(1), 1-11.

[37] Chai, T.J., Tan, Ch.S., Tang, H.K., et al., 2019. Compressive Strength and Water Absorption of Mortar Incorporating Silica Fume SSRG. International Journal of Civil Engineering. 6(8), 39-43.

[38] Olubajo, O.O., Osha, O.A., El-Nafaty, U.A., et al., 2017. A study on Coal bottom ash and limestone effects on the hydration and physico-mechanical properties of ternary cement blends. Ph.D. Thesis. Ababakar Tafawa Balewa University, Bauchi, Nigeria.

[39] Olubajo, O.O., Abubakar, J., Osha, O.A., 2020. The effect of eggshell ash and locust bean pod ash on the compressive strength of ternary cement. Path of Science. 6(3), 4001-4016. Available on website link: http://www.pos.org.

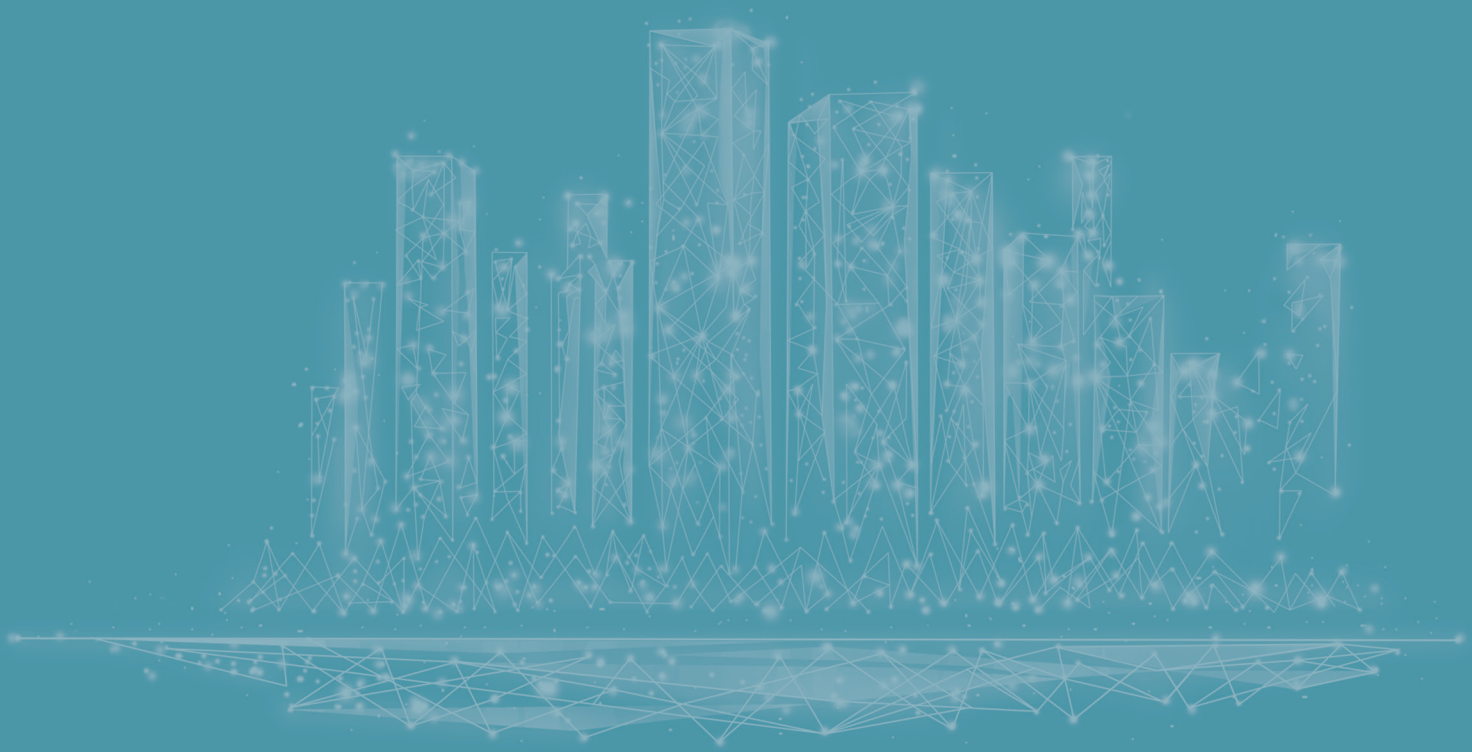

BILINGUAL
PUBLISHING CO.
Pioneer of Global Academics Since 1984

Tel:+65 65881289
E-mail: contact@bilpublishing.com
Website:ojs.bilpublishing.com

2630-5216
01
9 772630 521224